resulting in deactivation [18]. Development of cell matrices that maintain the activity of growth factors is thus required.

We have been studying 2-methacryloyloxyethyl phosphorylcholine (MPC) polymers synthesized as biomimetics in biomembrane structures [19–22]. MPC polymers have a surface that resists nonspecific protein adsorption and cell adhesion, i.e., "biofouling" [23,24]. MPC is a highly hygroscopic monomer and is useful for making hydrogels [25,26]. It has also been reported that hydrogels composed of MPC polymers can physisorb enzymes without deactivation [27]. Thus, MPC polymers may be a suitable matrix for physically entrapping growth factor without deactivation. Cell compatibility of MPC polymers has also been determined by measuring the amount of secreted IL-1β mRNA from adherent macrophage-like cells on polymer surfaces [28,29]. The mRNA expression from adherent cells on MPC polymer surfaces was significantly lower than that on conventional polymeric biomaterials. This property was the basis for studies of MPC polymer hydrogels as materials for tissue engineering [30,31].

In this study, a novel porous biodegradable MPC polymer hydrogel cross-linked with polyphosphoesters was prepared with a gas forming technique. The favorable characteristics of the hydrogels involve optimum mechanical properties, controllable biodegradability, and cell compatibility. Well-structured porous hydrogels were prepared and characterized, and cell cultivation in the hydrogels was also examined.

2. Materials and methods

2.1. Materials

MPC (Fig. 1) was synthesized by previously reported methods [32]. 2-Propanol, tetrahydrofurane (THF), and triethylamine (TEA) were obtained from Kanto Chemical, Co., Inc., Tokyo, Japan and purified by distillation. Poly[2-isopropyl-2-oxo-1,3,2-dioxaphospholane (IPP)-*co*-2-(2-oxo-1,3,2-dioxaphospholoyloxy)ethyl methactylate (OPEMA)] (PIOP) was synthesized by ring-opening polymerization using triisobutyl aluminum as an initiator (Scheme 1) [27,33]. The chemical structure of PIOP was confirmed by a ^{1}H NMR (α-500, JEOL, Tokyo, Japan). The average number molecular weight of PIOP was determined by gel-permeation chromatography (GPC) through a Shodex KF-803 column using a calibration curve based on linear polystyrene standards. The molecular weight of PIOP was 1.1×10^4 ($M_w/M_n = 1.1$). The calculated number of OPEMA units in a PIOP chain was 2.02.

Citric acid anhydrous and potassium hydrogen carbonate ($KHCO_3$) were purchased from Nakalai Tesque, Inc., Kyoto, Japan. For making the size of the $KHCO_3$ uniform, the salt was passed through a sieve with holes of (A) 500–300, (B) 300–250, and (C) 250–150 μm diameter before use. Other chemicals were purchased from Sigma-Aldrich Inc. and used without further purification.

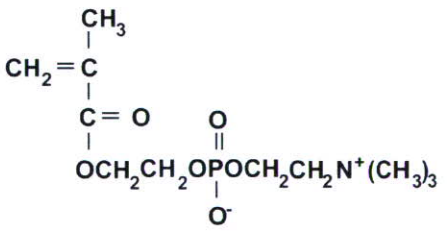

Fig. 1. Structure of MPC.

2.2. Preparation of hydrogels

Porous hydrogels were prepared using the following gas-forming process [34]. The desired PIOP, MPC, and 2,2-azobisisobutyronitrile (AIBN) were dissolved in ethanol. Then, argon gas was bubbled through the solution to eliminate oxygen. A monomer solution (0.5 mL) containing $KHCO_3$ (1.22 g) was poured into polyethylene molds (ϕ 15 mm) and incubated at 60 °C for 6 h under an argon gas atmosphere to obtain polymer gels. The gels were soaked in ethanol for 3 days to remove unreacted monomers. The top and bottom surfaces of each gel were sliced off and the balance of the gel was put in 50 mL of 3.0 mol/L citric acid solution for 12 h. The hydrogels were then washed for 24 h with distilled water that was changed several times. Hydrogels prepared without porogen salts were used for reference.

2.3. Physical properties of hydrogels

The hydrogels were cut into standard disc shapes 15 mm in diameter × 3 mm thick. The disks were measured with a rheometer (Rheograph Micro, Toyo Seiki Seisaku-sho, Ltd., Tokyo, Japan). The testing sample was horizontally loaded and tightly immobilized between double parallel plates. Sliding displacements on the sample–plate interfaces could not occur. A torsional stress was provided by rotation of the upper plate and determined by a transducer in the upper plate fixture.

The percent of porosity of the hydrogels was measured in the swollen state in water using Archimedes' principle [35]. Individual scaffolds were cut into standard disc shapes 15 mm in diameter × 3 mm thick and placed in a vial filled with 5 mL water (M_1) under negative pressure for 2–3 min. The total weight following complete scaffold immersion (M_2) was recorded. The hydrogels were then removed with the water trapped in the pores, and the weight (M_3) of the water left in the vial was recorded.

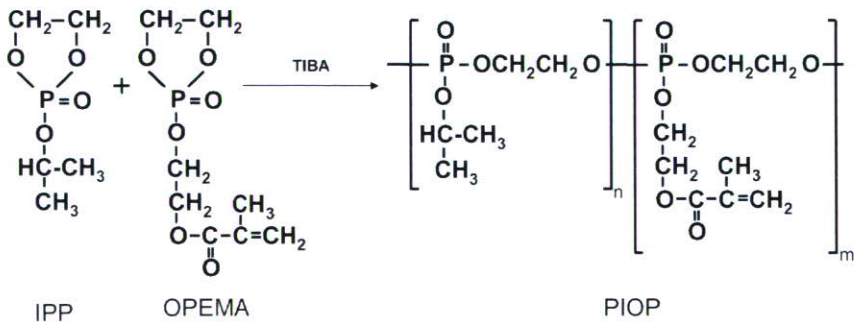

Scheme 1. Synthetic route of PIOP.

The porosity of the hydrogels was based on the following equation:

$$\text{Porosity}\ (\%) = [(M_1 - M_3)/M_T] \times 100 \quad (1)$$

where M_T ($= M_2 - M_3$) is the total weight of the porous hydrogels.

The porous structure of the lyophilized hydrogels was observed by scanning electron microscopy (SEM; JEOL, JSM-5400, Tokyo, Japan).

2.4. Swelling and hydrolytic dissolution behaviors and enzymatic digestion of hydrogels

A lyophilized hydrogel [15 mm (diameter) × 3 mm (thick)] was placed in a bag made of nylon mesh. The bag was soaked in a glass vial containing 100 mL of distilled water or a basic pH aqueous solution (pH 11; 0.10 mol/L Na_2HPO_4, 0.10 mol/L) and stored at 37 °C under gentle shaking. The weight of the nylon mesh bag was measured after given periods, and the swelling ratio of the gel was calculated from the following equation:

$$\text{Swelling}\ (\%) = [(W_s - W_0)/W_0] \times 100, \quad (2)$$

where W_0 and W_s are the weight of the lyophilized gel and that of the swollen gel, respectively.

To evaluate enzymatic digestion of the hydrogel, the nylon mesh bags containing the lyophilized hydrogel were soaked in Tris buffer solution (pH 9.0) containing alkaline phosphatase (ALP; Sigma-Aldrich Inc., St. Louis, MO, USA) at 37 °C. The swelling ratio of the hydrogel was determined as described. The solution was changed every 2 days to maintain the pH and ALP activity.

2.5. Physical absorption of growth factor in hydrogel

A lyophilized porous hydrogel was immersed into phosphate-buffered saline solution [PBS (pH 7.4), Sigma-Aldrich Inc., St. Louis, MO, USA] containing 1 μg basic fibroblast growth factor (bFGF) (F0291, Sigma-Aldrich Inc., St. Louis, MO, USA) for 24 h at 4 °C. The hydrogel was then rinsed with PBS twice and lyophilized again. To determine the total amount of growth factor physically absorbed in the hydrogels, the hydrogels were soaked in distilled water and disintegrated by means of ultrasonication. The solution was centrifuged to precipitate broken hydrogels. The concentration of growth factor in the supernatant was determined by enzyme-linked immunosorbent assay (ELISA; Quantikine Human FGF Basic Immunoassay; R&D Systems, Minneapolis, MN, USA).

2.6. Cell culture experiment

Mouse osteoblastic cells (MC3T3-E1) purchased from Riken Cell Bank were used because they are a well-characterized osteoblast-like cell line, which can serve as models for osteoblasts. The MC3T3-E1 cells were maintained in a culture media (α-MEM, GIBCO®, Invitrogen Corporation, Grand Island, NY, USA) with 10% fetal bovine serum at 37 °C in a humidified atmosphere of air containing 5% CO_2. The contents of the flasks for cell maintenance were detached by trypsin treatment, and a cell suspension containing 1.0×10^4 cells/mL in culture medium was prepared.

A porous hydrogel was cut into 5 mm × 5 mm × 2 mm and soaked in a disinfectant solution (70% ethanol in sterile water). After being sufficiently rinsed with sterile water, the hydrogel was lyophilized and incubated in bFGF/PBS. The hydrogel was rinsed with PBS, lyophilized again, and placed in a test tube kept at reduced pressure. The suspension of the MC3T3-E1 cells (1.0×10^4 cell/mL) was introduced into the test tube and stored until the gel was saturated. The hydrogel was transferred to a 24-well tissue culture plate and incubated in culture medium at 37 °C with 5% CO_2. The viability of adherent MC3T3-E1 cells in the hydrogel was investigated with a LIVE/DEAD® Viability/Cytotoxicity kit (Molecular Probes, OR, USA). After 24- and 96-h cultivation of the MC3T3-E1 cells in the hydrogel, the hydrogel was rinsed twice with fresh medium. The cells in the hydrogel were then stained with 1 μM calcein dye and 2 μM ethidium homodimer-1 (EthD-1) dye. The samples were incubated for 15 min at 37 °C and observed by phase-contrast and fluorescence microscopy (IX-70, OLYMPUS, Tokyo, Japan).

Fibronectin produced by the MC3T3-E1 cells in the hydrogel was observed by immunostaining. The cell-cultivated hydrogels were soaked in 1 wt% bovine serum albumin (BSA; Sigma-Aldrich Inc., St. Louis, MO, USA) in PBS solution, which was used as a blocking reagent to inhibit any undesirable reactions and nonspecific adsorption with following antibodies. The hydrogels were then incubated with primary antibodies (anti-mouse fibronectin rabbit polyclonal antiserum and anti-bovine fibronectin rabbit polyclonal antiserum; Life Technologies, Inc., MD, USA) for secreted fibronectin, rinsed with PBS, and then incubated with rhodamine-conjugated secondary antibody (Chemicon® International, Inc., Temecula, CA, USA). The hydrogels were then sufficiently rinsed with PBS. Mouse fibronectin in the hydrogel scaffolds was observed with a laser-scanning microscope (LSM 510 META, Zeiss, Jena, Germany).

The number of cells in each hydrogel disk was determined by measuring the DNA extracted from the cells. After cultivation for various durations, the hydrogels were immersed in 0.5 mL of TE buffer (10 mM Tris–HCl, 1 mM EDTA, pH 7.5) at 37 °C. To break up the cells in the hydrogel, the hydrogel was frozen and thawed three times. After removing the debris of the hydrogels and other impurities by centrifugation, the amount of DNA was determined by the use of a PicoGreen® assay kit (Molecular Probes, OR, USA). The PicoGreen-DNA complex was detected at a fluorescein excitation/emission wavelength of 485/538 nm using a multiwell plate reader (Wallac 1420 ARVOsx, PerkinElmer, Turku, Finland). The total amount of DNA in the sample was determined by using the standard provided in the kit.

2.7. Statistical analysis

The data are represented as the mean ± the standard deviation (SD). Statistical comparisons were performed with one-way ANOVA using SPSS® 10.0 (SPSS, Inc.).

3. Results and discussion

3.1. Preparation of hydrogels

The versatility of chemically synthesized polymers enables the fabrication of hydrogels with different features (e.g., form, porosity, pore size, rate of degradation, and mechanical property) to match tissue-specific applications. The synthetic conditions and characterizations of the hydrogels were summarized in Table 1.

Fig. 2 shows macroscopic pictures of the swollen hydrogels prepared in this study. The hydrogels (G1, G2, and G3) shown in Fig. 2a were prepared without porogen salts. When the cross-linking density was low, the hydrogels have highly stretched network, which was experimentally observed as a large transparent appearance. With an increase in the composition of PIOP, the size of the hydrogels decreased and its transparency became poor because the close distance of the PIOP molecules. Fig. 2b shows porous hydrogels (G1A, G2A, and G3A) prepared with the largest porogen salts ($\phi = 300$–500 μm). The effect of PIOP composition on the macroscopic form was similarly observed as in Fig. 2a. This result indicates that PIOP works as a macromolecular cross-linking reagent in the preparation of hydrogels. Many small bubbles are observed in the hydrogels prepared with porogen salts. From macroscopic observation, the difference in the inner structure between G1 and G1A is clarified.

Table 1
Synthetic condition and properties of hydrogels

Code	PIOP:MPC (%)	Potassium hydrogen carbonate size range (μm)	Swelling ratio (%)	Elastic modulus ($\times 10^4$ Pa)	Porosity (%)
G1	0.5:99.5	—	1519±208	2.47±0.47	95.0±0.3
G1A	0.5:99.5	500–300	1576±191	0.06±0.01	98.4±0.4
G1B	0.5:99.5	300–250	1549±502	0.05±0.01	98.2±0.1
G1C	0.5:99.5	250–150	1547±665	0.04±0.00	97.8±0.2
G2	1:99	—	804±128	3.08±0.77	92.7±0.6
G2A	1:99	500–300	963±129	0.18±0.01	96.4±0.3
G2B	1:99	300–250	957±153	0.21±0.02	96.5±0.1
G2C	1:99	250–150	977±26	0.26±0.01	96.7±0.2
G3	2.5:97.5	—	357±103	10.10±3.26	86.0±1.3
G3A	2.5:97.5	500–300	518±40	2.61±0.23	96.2±0.1
G3B	2.5:97.5	300–250	523±183	2.61±0.25	95.8±0.1
G3C	2.5:97.5	250–150	512±133	2.65±0.01	94.8±0.2

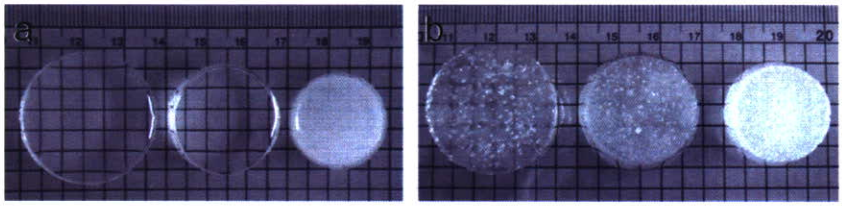

Fig. 2. Macroscopic pictures of swollen hydrogels. (a) Hydrogels without porogen salts (G1, G2, and G3) (b) Hydrogels with porogen salts (G1A, G2A, and G3A) after 24 h equilibration in water.

3.2. Characterization of highly porous hydrogels

Table 1 summarizes the physical properties of hydrogels. The swelling ratio was determined by soaking hydrogels in distilled water for 24 h and calculated with Eq. (2). The ratio was decreased significantly with an increase in the PIOP composition in hydrogels. The effect of the porous structure on the swelling of hydrogels with a higher cross-linking density was clearly observed.

The elastic modulus was strongly influenced by porosity and composition of PIOP, but not by the size of the porogen salts, as shown in Table 1. By changing the PIOP composition from 0.5 to 2.5 mol%, the elastic modulus of hydrogels was increased from $2.47\pm0.47\times10^4$ Pa (G1) to $10.10\pm0.10\times10^4$ Pa (G3) ($p = 0.0003$). The elastic modulus was significantly reduced by using porogen salts. When the composition of PIOP was 0.5 mol%, the modulus was reduced up to $0.06\pm0.01\times10^4$ Pa (G1A), which is about 2% of the modulus of hydrogel G1. In contrast, the elastic modulus of the G3A hydrogels containing 2.5 mol% PIOP was $2.66\pm0.01\times10^4$ Pa, and PIOP is effective in maintaining mechanical property after formation of the pores. In tissue engineering, hydrogel materials should provide mechanical support for the tissue as well as transmit mechanical stimuli. These mechanical requirements vary. Therefore, hydrogel materials must possess tailorable mechanical properties to suit given applications [36].

The porosity of hydrogels was also influenced by PIOP composition, decreasing with an increase in PIOP. By a gas-forming process, the porosity of hydrogels effectively increased. When the PIOP composition was 2.5 mol%, which is the highest cross-linking density, the effect of salt size on the porosity of the hydrogels was observed. Fig. 3 shows cross-sectional morphologies of the lyophilized hydrogels. These pictures correlate well with the porosity, as shown in Table 1. While microporous structures (<100 μm) were observed in hydrogel G1 prepared without porogen salts, the pore size decreased with an increase in PIOP composition and the pores almost disappeared in hydrogel G3. These pores look independent of each other, that is, not connected. In contrast, a highly porous structure was observed in the hydrogels prepared by a gas-forming technique. The pore sizes could be controlled by the size of the porogen salt. The pores appeared well interconnected to each other throughout the lyophilized hydrogels. There have been several reports describing the effect of pore size of the scaffold on cell ingrowth [37–40]. The optimal condition has not yet been identified because cell growth is affected by complex factors. However, well-controlled pore size is important in the design of a cellular matrix.

3.3. Hydrolytic dissolution

Fig. 4 shows the time dependence of the degree of hydration of the hydrogels soaked in pH 11 aqueous

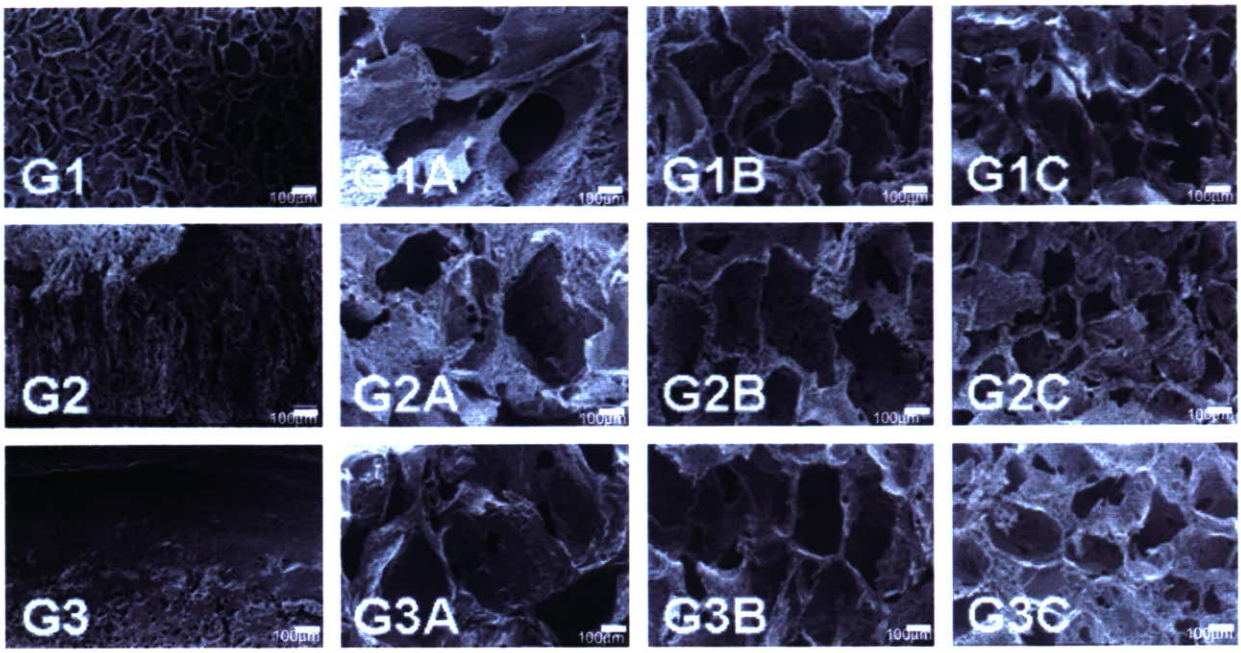

Fig. 3. Cross-sectional micrographs of lyophilized hydrogels.

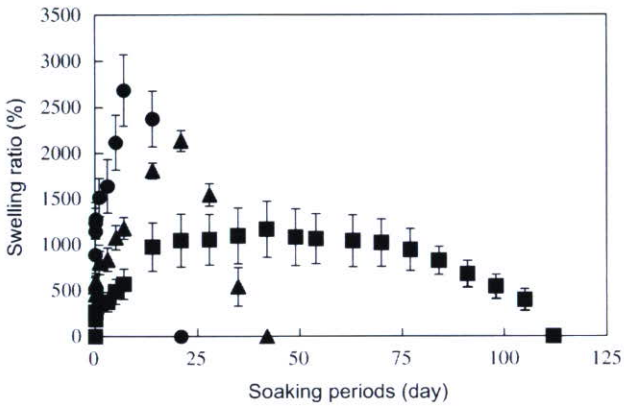

Fig. 4. Hydrolytic dissolution behavior as a function of time for hydrogels in basic aqueous solution (pH 11.0) at 37 °C; (●) G1, (▲) G2, (■) G3. Each point represents the average of three samples.

media. Although the basic condition used (pH 11.0) is not a physiological condition, we chose the optimal pH to characterize the degradation behavior of polyphosphates in a relatively short period. Penczek and coworkers reported the hydrolysis of poly(methylethylene phosphate) in the range from pH 1 to pH 12.63. Under basic conditions, the rate of hydrolysis of the main chain (k_m) was dramatically faster ($1.32 \times 10^{-5}\,s^{-1}$ at pH 11.16) than that under acidic conditions ($1.14 \times 10^{-8}\,s^{-1}$ at pH 3.78) [41]. The composition of PIOP influenced the swelling and hydrolytic dissolution periods. The hydrogel swelled quickly and the swelling ratio was stable after soaking for 1 day. The ratio gradually increased again after 3 days and the maximum swelling ratio of hydrogels G1, G2, and G3 was observed after 7, 22, and 42 days, respectively. This increment of the swelling ratio may be the hydrolysis of the phosphate linkage in the hydrogels and result in decreasing the cross-linking density. After reaching the maximum point of the swelling ratio, the hydrogels began to dissolve and their weight decreased. Changing the composition of PIOP can control the rate of hydrolysis.

We have reported on the pH dependence of hydrolysis of hydrogels previously [27]. In acidic (pH 3.0) and physiological (pH 7.4) conditions, the hydrolysis was much slower than that in basic (pH 11.0) condition. The behavior correlated well with the hydrolysis of PIOP. The degradation products determined by ^{1}H NMR and GPC consisted of poly(MPC) and low molecular weight substances [27].

Fig. 5 is a comparison of the degradation profile of the hydrogels prepared with or without porogen salts. The porous hydrogel, G1A, degraded faster than the G1 hydrogel. The aqueous media may diffuse easily in a porous hydrogel due to interconnecting pores. The reduction of degradation periods due to the porous structure was also observed on G2A and G3A.

3.4. Enzymatic digestion of hydrogels

ALP is an important enzyme produced in bone and liver cells. It catalyzes the hydrolysis of phosphate groups from monophosphate ester substrates mostly found in an alkaline state with a pH of 9 [42]. While Zhao et al. [43] reported that synthetic polyphosphates and polyphosphoesters are enzymatically degradable, the process was not described in detail. The concentration of ALP for the degradation study was adjusted to 72.5 and 220 U/L, which is the concentration in healthy

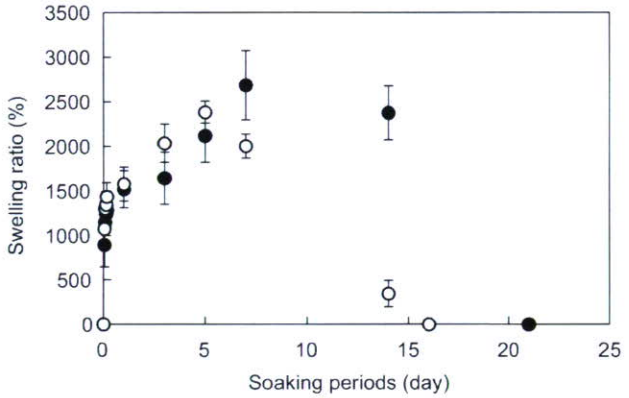

Fig. 5. Effect of porous structure of hydrogels on the hydrolytic dissolution in basic aqueous solution (pH 11.0) at 37 °C. (●) G1, (○) G1A. Each point represents the average of three samples.

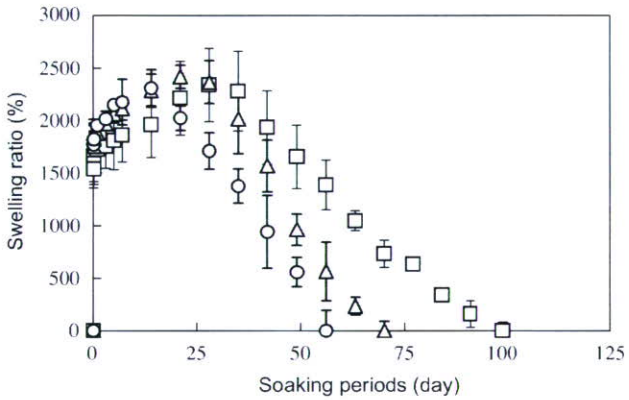

Fig. 6. Enzymatic degradation as a function of time for hydrogel G1A in ALP aqueous solution at 37 °C; [ALP] = 0 U/L (□), 72.5 U/L (△), 220 U/L (○). Each point represents the average of three samples.

adults and children, respectively [44,45]. Fig. 6 is an enzymatic degradation profile of G1A hydrogels by changing the concentration of ALP. G1A took about 100 days to reach complete dissolution at pH 9.0. The degradation was accelerated with a higher concentration of ALP, and G1A completely degraded after 60 days in 220 U/L of ALP. The degradation period was shortened with an increase in the concentration of the enzyme and the digestion of a hydrogel might be regulated by varying the density of cells secreting an enzyme in the hydrogel.

3.5. Physical absorption of bFGF in hydrogels

Osteoblasts that synthesize FGFs are produced by bone cells, increase the proliferation of osteoblastic cells, and stimulate bone formation and fracture healing [46–49]. FGFs are potent regulators of gene expression in cells of osteoblastic lineage, playing roles in skeletal development and facture repair [50].

The amount of bFGF physically absorbed in hydrogels G1A, G2A, and G3A were 11.9, 13.9, and 17.5 ng, respectively. By increasing the cross-linking density of the hydrogel, the amount of bFGF in hydrogels was increased. We have reported that the interaction of MPC unit interaction with proteins is very weak and nonspecific fouling of proteins on the MPC polymer surface is significantly reduced [24]. PIOP then acts to induce absorption of bFGF in a hydrogel. The hydrophobic nature of PIOP might also influence the interaction of proteins.

To understand the absorption phenomena of bFGF in a hydrogel, the released profile of bFGF was determined by soaking the hydrogel in culture medium. Lyophilized hydrogels containing bFGF were soaked in cell culture medium (1 mL) and the medium (100 μL) was collected at various periods. The concentration of bFGF in the medium was measured by ELISA. Fig. 7 shows the release profile of bFGF from hydrogels with different cross-linking density. In every case, an abundance of bFGF was released during the first 24 h. Even burst release in the first 24 h, the effect of PIOP composition on the percentage

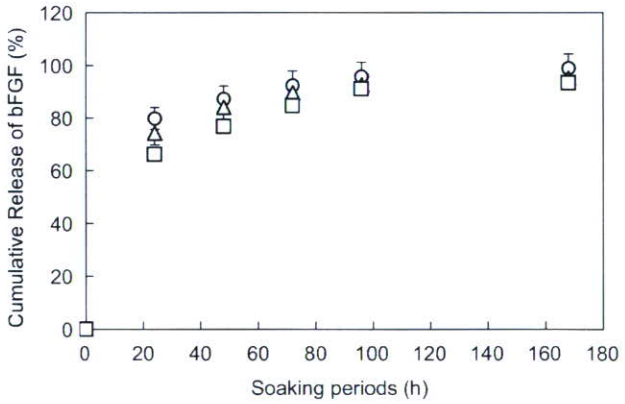

Fig. 7. Release profile of bFGF from hydrogels at 37 °C. (○) G1A, (△) G2A, (□) G3A. Each point represents the average of the three samples.

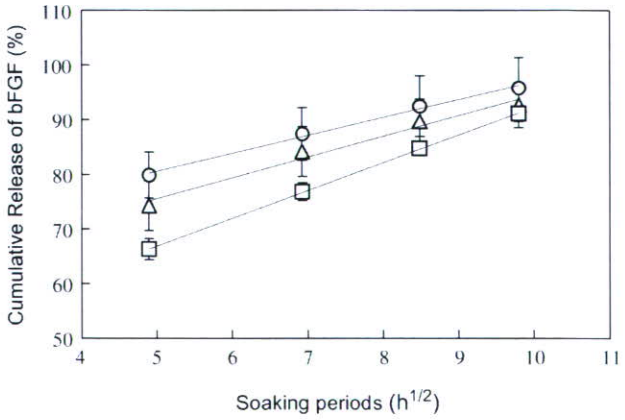

Fig. 8. The released percent of bFGF from a hydrogel described as a function of the square root of time. (○) G1A, (△) G2A, (□) G3A.

released was observed, that is, 80.0% in G1A and 66.3% in G3A. After a soaking period of 24 h, the rate of release of bFGF from the hydrogels decreased. G1A and G3A released 98.9% and 93.4% of bFGF for 168 h, respectively. Fig. 8 shows the percentage of released bFGF as a function of the square root of time. The plots linearly increased with the square root of time and the release mechanism was chiefly that of diffusion [51]. While the fraction of hydrogels affected the release profile at the early stage, almost of absorbed bFGF was released for a week. The irreversible adsorption of bFGF on hydrogels might not be occurred.

3.6. Cell viability and proliferation in hydrogels

MC3T3-E1 is a clonal osteogenic cell line derived from neonatal mouse calvaria. These cells are well characterized and provide a homogeneous source of osteoblastic cells for study. They were encapsulated in various biomaterial networks and remained viable [52]. MC3T3-E1 cells express high levels of ALP and differentiate into osteoblasts that can form calcified bone tissue in vitro [53]. The response of MC3T3-E1 cells to many growth factors and hormones mimics that of primary cultures of rodent osteoblastic cells.

The cell viability of MC3T3-E1 cells in G3A hydrogels was evaluated by "Live/Dead" dye-staining, as shown in Fig. 9. All cells cultured in a hydrogel for 24 and 96 h with bFGF were stained with calcein but not with EthD-1. To determine the dependability of this assay, the hydrogel was treated with 1×10^{-3} M sodium dodecyl sulfate (SDS) solution for 30 min. After SDS treatment, every cell in the hydrogel was stained with EthD-1. The result of the staining assay indicated that the hydrogel did not have any adverse effects on cell viability.

Fig. 10 shows merged micrographs for fibronectin secretion of MC3T3-E1 cells cultured in G1A and G3A hydrogels for 96 h as determined by an immunostaining method. Because of poor transparency, the pictures of G3A were not clear. To identify the fibronectin secreted from the cells, a rhodamine-conjugated secondary antibody was used. Stained fibronectin was observed at the outline of the cells in hydrogel G1A. When the growth factor was incorporated in the hydrogel, the secretion of fibronectin from the cell tended to be more outstanding. Although the shape of the cells in hydrogel G3A is not clear, the number of cells is greater than that in hydrogel G1A. Much more fibronectin was observed in the hydrogel G3A.

Fig. 11 shows the time-dependent concentration of the DNA produced from the MC3T3-E1 cells in porous hydrogels. The concentration increment of DNA corresponds to the proliferation of cells in a hydrogel. On every sample condition, the amount of DNA significantly increased ($p<0.05$) with an increased cultivation time. At 168 h-cultivation, the amount of DNA collected was

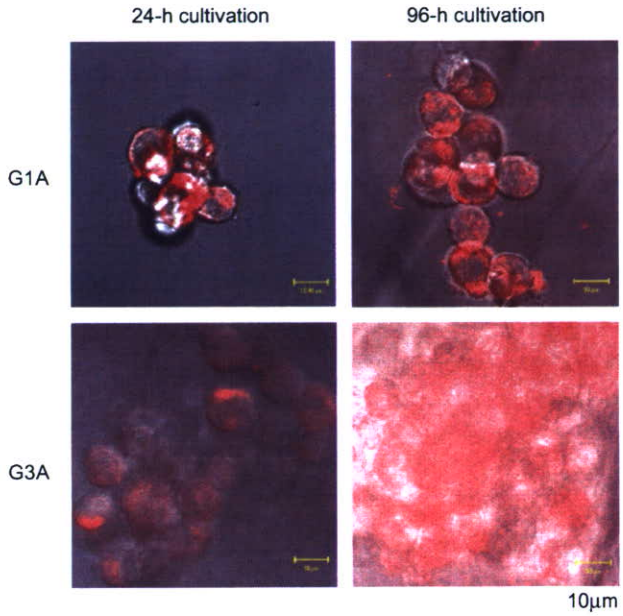

Fig. 10. Fibronectin secreted from MC3T3-E1 cells in hydrogels.

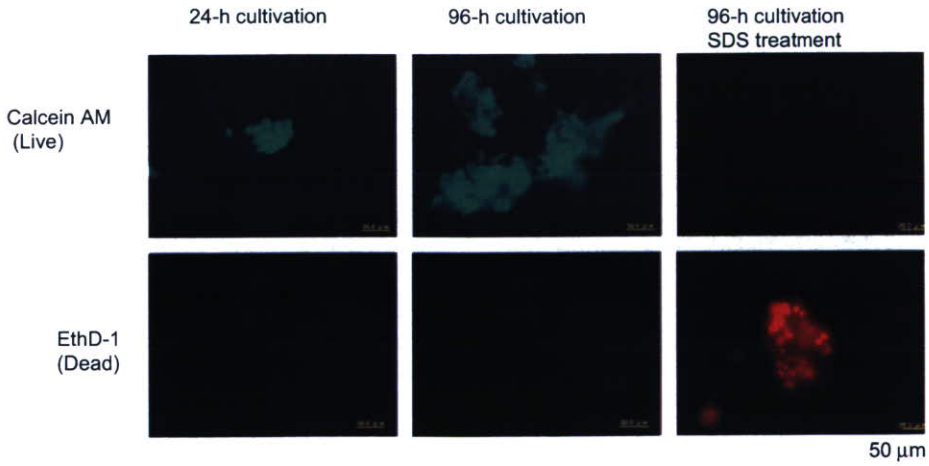

Fig. 9. Fluorescence micrographs of viability of MC3T3-E1 cells in hydrogel G3A after culture of 24 and 96 h with bFGF.

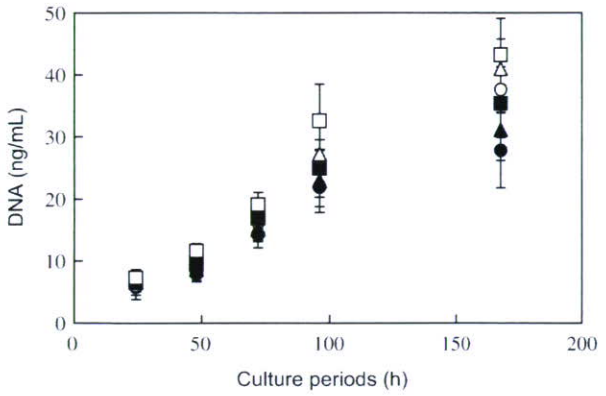

Fig. 11. Kinetics of MC3T3-E1 cell proliferation in hydrogels. (○) G1A, (△) G2A, (□) G3A with bFGF; (●) G1A, (▲) G2A, (■) G3A without bFGF.

significantly higher from G3A ($p = 0.036$) in comparison to G1A. Therefore, the density of PIOP influenced cell proliferation. When the bFGF was incorporated in to a hydrogels, the rate of cell proliferation relatively increased with an increase in the concentration of PIOP ($p = 0.017$ and 0.107 G1A vs. G3A after culture for 96 and 168 h, respectively). While MPC polymer provides a suitable condition for maintaining cell viability, this polymer is not effective for inducing cell adhesion on the surface [21]. Polyphosphate may induce cell adhesion and proliferation in a hydrogel. Wang and coworkers have recently reported that poly(ethylene glycol) (PEG) hydrogel having a phosphoester linkage promotes gene expression of bone-specific markers and secretion of ALP, osteocalcin, and osteonectin protein from marrow-derived mesenchymal stem cells [54]. They also indicated that mineralization of the hydrogel was preferably constructed compared with that of PEG hydrogel, which has no phosphoester linkage. Polyphosphate linkage might have a good potential impact on bone engineering applications.

The number of cells cultured in hydrogel G3A, which has the highest incorporated concentration of the growth factor, was preferentially increased with culture periods ($p = 0.010$ at culture for 96 h and $p = 0.033$ at culture for 168 h vs. G3A without bFGF), as shown in Fig. 11. It has been reported that the in vitro half-life of bFGF activity is approximately 12 h at physiological pH and temperature [55]. bFGF was entrapped in the hydrogels to enhance the stability of the growth factor during release because the hydrogels have MPC units that absorb proteins on the MPC polymer that did not change the conformation compared with native protein [24]. The effect of growth factor in every hydrogel on cell proliferation was observed and the activity of growth factor incorporated in hydrogels was not diminished after lyophilization. The porous hydrogels prepared in this study provide a suitable environment to maintain growth factor activity. When the growth factor was incorporated in the hydrogel, the rate of cell proliferation increased with an increase in cross-linking density. This result indicates that both the growth factor and the polyphosphoester cross-linker affect cell proliferation.

4. Conclusion

Highly porous hydrogels consisting of MPC polymers cross-linked with polyphosphoesters were prepared by a gas-forming process using porogen salts. The hydrogels were degraded by hydrolysis of cross-linking polyphosphoesters. Degradation behavior could then be controlled by the cross-linking density and porous structure. The degradation of the hydrogels was also accelerated with the introduction of ALP. When MC3T3-E1 cells were incorporated in the hydrogels, the viability of the cells was preferentially maintained and no dead cells were observed after culture for 96 h. Growth factors physically absorbed in the hydrogels worked well and they effectively improved cell proliferation. The polyphosphoester cross-linker also affects cell proliferation and function. The porous hydrogels prepared in this study perform as novel cellular matrices, which might be useful for cell and tissue engineering applications.

Acknowledgements

This work was supported by the Japan Society for the Promotion of Science (Grant-in-aid for Encouragement of Young Scientists (18681018)). We gratefully acknowledge the valuable discussion provided by Dr. Tooru Ooya of Toyama Prefectural University.

References

[1] Lin ASP, Barrows TH, Cartmell SH, Guldberg RE. Microarchitectural and mechanical characterization of oriented porous polymer scaffolds. Biomaterials 2003;24:481–9.
[2] Hennink WE, van Nostrum CF. Novel crosslinking methods to design hydrogels. Adv Drug Deliv Rev 2002;54:13–36.
[3] Jeong B, Kim SW, Bae YH. Thermosensitive sol-gel reversible hydrogels. Adv Drug Deliv Rev 2002;54:37–51.
[4] Tsang VL, Bhatia SN. Three-dimensional tissue fabrication. Adv Drug Deliv Rev 2004;56:1635–47.
[5] Pratt AB, Weber FE, Schmoekel HG, Muller R, Hubbell JA. Synthetic extracellular matrices for in situ tissue engineering. Biotechnol Bioeng 2004;86:27–36.
[6] Libiszowski J, Kaluzynski K, Penczek S. Polymerization of cyclic esters of phosphoric acid. VI. Poly(alkylethylene phosphates). Polymerization of 2-alkoxy-2-oxo-1,3,2-dioxaphospholans and structure of polymer. J Polym Sci A Polym Chem 1978;16:1275–83.
[7] Pretula J, Kaluzynski K, Penczek S. Synthesis of poly(alkylene phosphates) with nitrogen-containing bases in the side Chain. 1.N- and C-substituted imidazoles. Macromolecules 1986;19:1797–9.
[8] Richards M, Dahiyat BI, Arm DM, Lin S, Leong KW. Interfacial polycondensation and characterization of polyphosphates and polyphosphonates. J Polym Sci A Polym Chem 1991;29:1157–65.
[9] Pretura J, Kaluzynski K, Szymanski R, Penczek S. Transesterification of oligomeric dialkyl phosphonates, leading to the high-molecular-weight poly-H-phosphonates. J Polym Sci A Polym Chem 1999; 37:1365–81.

[10] Myrex RD, Farmer B, Gray GM, Wright YJ, Dees J, Bharara PC, et al. ^{31}P and ^{1}H NMR studies of the transesterification polymerization of poly phosphonate oligomers. Euro Polym J 2003; 39:1105–15.
[11] Wen J, Zhuo RX. Enzyme-catalyzed ring-opening polymerization of ethylene isopropyl phosphate. Macromol Rapid Commun 1998; 19:641–2.
[12] Wan AC, Mao HQ, Wang S, Leong KW, Ong LK, Yu H. Fabrication of poly(phosphoester) nerve guides by immersion precipitation and the control of porosity. Biomaterials 2001;22: 1147–56.
[13] Wang J, Zhang PC, Lu HF, Ma N, Wang S, Mao HQ, et al. New polyphosphoramidate with a spermidine side chain as a gene carrier. J Control Release 2002;83:157–68.
[14] Huang SW, Wang J, Zhang PC, Mao HQ, Zhuo RX, Leong KW. Water-soluble and nonionic polyphosphoester: synthesis, degradation, biocompatibility and enhancement of gene expression in mouse muscle. Biomacromolecules 2004;5:306–11.
[15] Li Q, Wang J, Shahani S, Sun DD, Sharma B, Elisseeff JH, et al. Biodegradable and photocrosslinkable polyphosphoester hydrogel. Biomaterials 2006;27:1027–34.
[16] Heller J, Hoffman AS. Drug delivery system. In: Buddy DR, Allan SH, Frederick JS, Jack EL, editors. Biomaterials science. 2nd ed. San Diego: Elsevier; 2004. p. 628–48.
[17] Langer R, Vacanti JP. Tissue Eng Sci 1993;260:920–6.
[18] Westal FC, Rubin R, Gospodarowicz D. Brain derived fibroblast growth factor: a study of its inactivation. Life Sci 1983;33:2425–59.
[19] Iwasaki Y, Mikami A, Kurita K, Yui N, Ishihara K, Nakabayashi N. Reduction of surface-induced platelet activation on phospholipid polymer. J Biomed Mater Res 1997;36:508–15.
[20] Iwasaki Y, Sawada S, Nakabayashi N, Khang G, Lee HB, Ishihara K. The effect of the chemical structure of the phospholipid polymer on fibronectin adsorption and fibroblast adhesion on the gradient phospholipid surface. Biomaterials 1999;20:2185–91.
[21] Ishihara K, Ishikawa E, Iwasaki Y, Nakabayashi N. Inhibition of fibroblast cell adhesion on substrate by coating with 2-methacryloyloxyethyl phosphorylcholine polymers. J Biomater Sci Polym 1999; 10:1047–61.
[22] Iwasaki Y, Nakabayashi N, Ishihara K. Preservation of platelet function on 2-methacryloyloxyethyl phosphorylcholine-graft polymer as compared to various water-soluble graft polymers. J Biomed Mater Res 2001;57:72–8.
[23] Ishihara K, Oshida H, Endo Y, Ueda T, Watanabe A, Nakabayashi N. Hemocompatibility of human whole blood on polymers with a phospholipid polar group and its mechanism. J Biomed Mater Res 1992;26:1543–52.
[24] Ishihara K, Nomura H, Mihara T, Kurita K, Iwasaki Y, Nakabayashi N. Why do phospholipid polymers reduce protein adsorption? J Biomed Mater Res 1998;39:323–30.
[25] Nam KW, Watanabe J, Ishihara K. Characterization of the spontaneously forming hydrogels composed of water-soluble phospholipid polymers. Biomacromolecules 2002;3:100–5.
[26] Kimura M, Fukumoto K, Watanabe J, Takai M, Ishihara K. Spontaneously forming hydrogel from water-soluble random- and block-type phospholipid polymers. Biomaterials 2005;26:6853–62.
[27] Iwasaki Y, Nakagawa C, Ohtomi M, Ishihara K, Akiyoshi K. Novel biodegradable polyphosphate cross-linker for making biocompatible hydrogel. Biomacromolecules 2004;5:1110–5.
[28] Iwasaki Y, Sawada S, Ishihara K, Khang G, Lee HB. Reduction of surface-induced inflammatory reaction on PLGA/MPC polymer blend. Biomaterials 2002;23:3897–903.
[29] Sawada S, Sakaki S, Iwasaki Y, Nakabayashi N, Ishihara K. Suppression of the inflammatory response from adherent cells on phospholipid polymers. J Biomed Mater Res A 2003;1:411–6.
[30] Watanabe J, Eriguchi T, Ishihara K. Cell adhesion and morphology in porous scaffold based on enantiomeric poly(lactic acid) graft-type phospholipid polymers. Biomacromolecules 2002; 3:1375–83.
[31] Watanabe J, Ishihara K. Cell engineering biointerface focusing on cytocompatibility using phospholipid polymer with an isomeric oligo(lactic acid) segment. Biomacromolecules 2005;6:1797–802.
[32] Ishihara K, Ueda T, Nakabayashi N. Preparation of phospholipid polymers and their properties as polymer hydrogel membrane. Polym J 1990;22:355–60.
[33] Iwasaki Y, Komatsu S, Narita T, Akiyoshi K, Ishihara K. Biodegradable phosphorylcholine polymer hydrogels cross-linked with vinyl-functionalized polyphosphate. Macromol Biosci 2003;3: 238–42.
[34] Ichi T, Nitta K, Lee WK, Ooya T, Yui N. Preparation of porous hydrolyzable polyrotaxane hydrogels and their erosion behavior. J Biomater Sci Polym Ed 2003;14:567–79.
[35] Karageorgiou V, Kaplan D. Porosity of 3D biomaterial scaffolds and osteogenesis. Biomaterials 2005;26:5474–91.
[36] Stankus JJ, Guan J, Wagner WR. Fabrication of biodegradable elastomeric scaffolds with sub-micron morphologies. J Biomed Mater Res 2004;70A:603–14.
[37] Nehrer S, Breinan HA, Ramappa A, Young G, Shortkroff S, Louie LK, et al. Matrix collagen type and pore size influence behavior of seeded canine chondrocytes. Biomaterials 1997;18: 769–76.
[38] Itala AI, Ylanen HO, Ekholm C, Karlsson KH, Aro HT. Pore diameter of more than 100 microm is not requisite for bone ingrowth in rabbits. J Biomed Mater Res 2001;58:679–83.
[39] Salem AK, Stevens R, Pearson RG, Davies MC, Tendler SJ, Roberts CJ, et al. Interactions of 3T3 fibroblasts and endothelial cells with defined pore features. J Biomed Mater Res 2002; 61(2):212–7.
[40] O'Brien FJ, Harley BA, Yannas IV, Gibson LJ. The effect of pore size on cell adhesion in collagen-GAG scaffolds. Biomaterials 2005;26:433–41.
[41] Baran J, Penczek S. Hydrolysis of polyesters of phosphoric acid. 1. Kinetics and the pH profile. Macromolecules 1995;28:5167–76.
[42] Coburn SP, Mahuren JD, Jain M, Zubovic Y, Wortsman J. Alkaline phosphatase (EC 3.1.3.1) in serum is inhibited by physiological concentrations of inorganic phosphate. J Clin Endocrinol Metab 1998;83:3951–7.
[43] Zhao Z, Wang J, Mao HQ, Leong KW. Polyphosphoesters in drug and gene delivery. Adv Drug Deliv Rev 2003;5:483–99.
[44] Takeshita T, Tanaka H, Harasawa A, Kaminaga T, Imamura T, Furui S. Brown tumor of the sphenoid sinus in a patient with secondary hyperparathyroidism: CT and MR imaging findings. Rad Med 2004;22:265–8.
[45] Rafanan AL, Maurer J, Mehta AC, Schilz R. Progressive portopulmonary hypertension after liver transplantation treated with epoprostenol. Chest 2000;118:1497–500.
[46] Globus RK, Patterson-Buckendahl P, Gospodarowicz D. Regulation of bovine bone cell proliferation by fibroblast growth factor and transforming growth factor beta. Endocrinology 1988;123: 98–105.
[47] Globus RK, Poulet J, Gospodarowicz D. Cultured bovine bone cell synthesize basic fibroblast growth factor and store it in their extracellular matrix. Endocrinology 1989;124:1539–47.
[48] Mayahara H, Ito T, Nagai H, Miyajima H, Tsukuda R, Taketomi S, et al. In vivo stimulation of endosteal bone formation by basic fibroblast growth factor in rats. Growth Fact 1993;9:73–80.
[49] Kawaguchi H, Kurokawa T, Hanada K, Hiyama Y, Tamura M, Ogata E, et al. Stimulation of fracture repair by recombinant human basic fibroblast growth factor in normal and streptozotocin-diabetic rats. Endocrinology 1994;135:774–81.
[50] Kawaguchi H, Kurokawa T, Hanada K, Hiyama Y, Tamura M, Ogata E, et al. Stimulation of fracture repair by recombinant human basic fibroblast growth factor in normal and streptozotocin-diabetic rats. Endocrinology 1994;135:774–81.
[51] Park K, Shalaby WS, Park H. Biodegradable drug delivery systems. In: Park K, Shalaby WS, Park H, editors. Biodegradable hydrogels

for drug delivery. Lancaster: Technomic Publishing Company; 1993. p. 189–99.

[52] Burdick JA, Chung C, Jia X, Randolph MA, Langer R. Controlled degradation and mechanical behavior of photopolymerized hyaluronic acid networks. Biomacromolecules 2005;6:386–91.

[53] Choi JY, Lee BH, Song KB, Park RW, Kim IS, Sohn KY, et al. Expression patterns of bone-related proteins during osteoblastic differentiation in MC3T3-E1 cells. J Cell Biochem 1996; 61:609–18.

[54] Wang DA, Williams CG, Yang F, Cher N, Lee H, Elisseeff JH. Bioresponsive phosphoester hydrogels for bone tissue engineering. Tissue Eng 2005;11:201–13.

[55] Westal FC, Rubin R, Gospodarowicz D. Brain derived fibroblast growth factor: a study of its inactivation. Life Sci 1983;33:2425–59.

Available online at www.sciencedirect.com
ScienceDirect
Colloids and Surfaces B: Biointerfaces 57 (2007) 226–236
COLLOIDS AND SURFACES B
www.elsevier.com/locate/colsurfb

Surface modification with well-defined biocompatible triblock copolymers
Improvement of biointerfacial phenomena on a poly(dimethylsiloxane) surface

Yasuhiko Iwasaki [a,*], Mika Takamiya [a,c], Ryoko Iwata [a], Shin-ichi Yusa [d], Kazunari Akiyoshi [a,b]

[a] *Institute of Biomaterials and Bioengineering, Tokyo Medical and Dental University, 2-3-10 Kanda-surugadai, Chiyoda-ku, Tokyo 101-0062, Japan*
[b] *Center of Excellence Program for Frontier Research on Molecular Destruction and Reconstruction of Tooth and Bone, Tokyo Medical and Dental University, 2-3-10 Kanda-surugadai, Chiyoda-ku, Tokyo 101-0062, Japan*
[c] *Department of Chemistry, Faculty of Science, Toho University, 2-2-1 Miyama, Funabashi-shi, Chiba 274-8510, Japan*
[d] *Department of Materials Science and Chemistry, Graduate School of Engineering, University of Hyogo, 2167 Shosha, Himeji-shi, Hyogo 671-2280, Japan*

Received 12 November 2006; received in revised form 8 January 2007; accepted 3 February 2007
Available online 11 February 2007

Abstract

To improve interfacial phenomena of poly(dimethylsiloxane) (PDMS) as biomaterials, well-defined triblock copolymers were prepared as coating materials by reversible addition-fragmentation chain transfer (RAFT) controlled polymerization. Hydroxy-terminated poly(vinylmethylsiloxane-co-dimethylsiloxane) (HO–PV_lD_mMS–OH) was synthesized by ring-opening polymerization. The copolymerization ratio of vinylmethylsiloxane to dimethylsiloxane was 1/9. The molecular weight of HO–PV_lD_mMS–OH ranged from (1.43 to 4.44) × 10^4, and their molecular weight distribution (M_w/M_n) as determined by size-exclusion chromatography equipped with multiangle laser light scattering (SEC-MALS) was 1.16. 4-Cyanopentanoic acid dithiobenzoate was reacted with HO–PV_lD_mMS–OH to obtain macromolecular chain transfer agents (macro-CTA). 2-Methacryloyloxyethyl phosphorylcholine (MPC) was polymerized with macro-CTAs. The gel-permeation chromatography (GPC) chart of synthesized polymers was a single peak and M_w/M_n was relatively narrow (1.3–1.6). Then the poly(MPC) (PMPC)–PV_lD_mMS–PMPC triblock copolymers were synthesized. The molecular weight of PMPC in a triblock copolymer was easily controllable by changing the polymerization time or the composition of the macro-CTA to a monomer in the feed. The synthesized block copolymers were slightly soluble in water and extremely soluble in ethanol and 2-propanol.

Surface modification was performed *via* hydrosilylation. The block copolymer was coated on the PDMS film whose surface was pretreated with poly(hydromethylsiloxane). The surface wettability and lubrication of the PDMS film were effectively improved by immobilization with the block copolymers. In addition, the number of adherent platelets from human platelet-rich plasma (PRP) was dramatically reduced by surface modification. Particularly, the triblock copolymer having a high composition ratio of MPC units to silicone units was effective in improving the surface properties of PDMS.

By selective decomposition of the Si–H bond at the surface of the PDMS substrate by irradiation with UV light, the coating region of the triblock copolymer was easily controlled, resulting in the fabrication of micropatterns. On the surface, albumin adsorption was well manipulated.

Keywords: Phosphorylcholine polymer; PDMS; RAFT polymerization; Block copolymer; Surface modification; Non-fouling; Lubrication

1. Introduction

Poly(dimethylsiloxane) (PDMS) is one of the most valuable polymers for use in biomedical devices such as catheters, tracheoesophageal voice prostheses, finger joints, percutaneous devices, dentures, etc. [1]. One of the more recent trends in PDMS applications is microfluidic devices for biosensors or

* Corresponding author. Tel.: +81 3 5280 8022; fax: +81 3 5280 8027.
E-mail address: yasu.org@tmd.ac.jp (Y. Iwasaki).

0927-7765/$ – see front matter © 2007 Elsevier B.V. All rights reserved.
doi:10.1016/j.colsurfb.2007.02.007

biochips [2–5]. PDMS has flexibility, high gas permeability, processability, flexible surface chemistry, and optical transparency. However, the interface of the PDMS surface with the biological environment is inadequate, and non-specific biofouling, i.e., protein adsorption and cell adhesion frequently occurs on the surface [6–9]. Biofouling induces contamination, inflammation, infection, and the reduction of material function. Highly friction of PDMS surface is also unfavorable nature for medical applications. These disadvantages of PDMS are due to hydrophobicity of the surface, necessitating surface modification. The formation of a hydrophilic surface on PDMS by using oxidization [10,11] and hydrophilic polymers [12–14] is proposed as a method of solving interfacial problems. Poly(ethylene glycol) (PEG) is one of the principal polymer candidates for reducing non-specific fouling at the biointerface [15]. For PDMS, covalent bonding onto PDMS surfaces of PEG-functionalized silanes [16–18] or amine-functionalized silanes to further react with PEG-moieties [19,20] has generally been employed. PEGylation is very effective in reducing biofouling. However, cell adhesion was observed on surfaces after long-term exposure in a culture medium [21].

To obtain other types of reliable non-fouling surfaces, we have been studying 2-methacryloyloxyethyl phosphorylcholine (MPC) polymers synthesized as biomimetics in biomembrane structures [22–24]. There have been some reports describing the surface modification of PDMS with MPC. Plasma-induced graft polymerization was applied as a primary process [25,26]. However, this modification has limitations in increasing the surface composition of MPC units because the phosphorus concentration remained low compared with the theoretical amount calculated from the chemical structure of MPC. Goda et al. recently reported the photo-induced grafting of MPC on a PDMS surface [14]. They succeeded in improving the composition of the MPC units on the PDMS surface compared with plasma polymerization. Moreover, the surface friction of PDMS surface effectively reduced by the surface modification. Although surface modification with MPC polymers *via* the grafting process is valuable for achieving a non-fouling surface on PDMS, their use precludes accurate control of the polymer structure and specific equipment is required.

Surface-coating processes are more applicable as methods of surface modification. Generally, organic solvent is used for the surface modification of PDMS, and the coating of hydrophilic polymer on PDMS is difficult because the surface is hydrophobic and has a low surface energy. The surface modification of PDMS using polar solvent is still limited [27]. A precise molecular design of an MPC polymer having the desired solubility and anchors that have an affinity to the PDMS surface is needed for reliable surface modification.

To produce well-defined polymers, controlled "living" radical polymerization has been explored [28]. Atom transfer radical polymerization (ATRP) and reversible addition-fragmentation chain transfer (RAFT) polymerization are very useful for achieving this process because they can be applied to a wide variety of monomers [29–35]. We have prepared poly(MPC) (PMPC) brush on a silicon wafer *via* ATRP and clarified that plasma protein adsorption and cell adhesion were effectively reduced on the surface with a polymer brush thickness of only 5 nm [36]. While the use of well-defined polymer brush with ATRP is considerable theoretical and experimental interests in control of surface properties, some specific conditions for the reaction are needed and still difficult to use as a common method of surface modification.

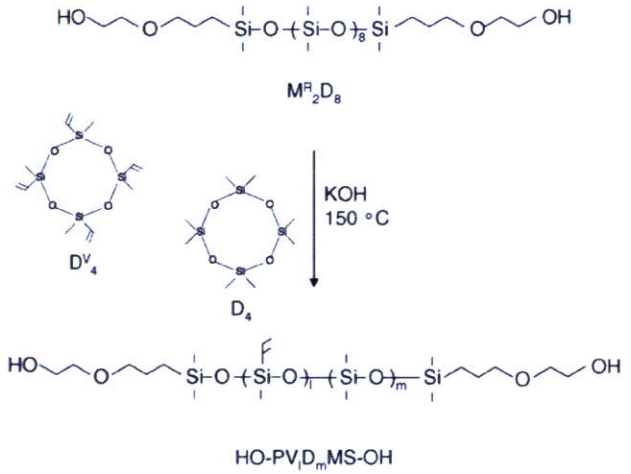

Scheme 1. Synthetic route of hydroxy-terminated poly(vinylmethylsiloxane-co-dimethylsiloxane) (OH–PV_lD_mMS–OH).

This paper primary reports surface modification of PDMS with well-defined ABA-type triblock copolymers composed of poly(MPC) (PMPC) blocks (A) and central silicone blocks (B) with anchoring vinyl groups by using a simple coating process. We also determine the effects of structures of the copolymers on the surface properties and clarify that the block copolymers have great power to improve interfacial phenomena of PDMS as biomaterials.

2. Materials and methods

2.1. Materials

Dicyclohexylcarbodiimide (DCC) and 4-dimethylaminopyridine was purchased from Kanto Chemical Co. Ltd., Japan and used without further purification. 4-Cyanopentanoic acid dithiobenzoate was synthesized according to the method reported by McCormick and co-workers [34]. Octamethylcyclotetrasiloxane (D_4), tetramethyl tetravinyl cyclotetrasiloxane (D^V_4), and hydroxyethoxypropyl dimethylsilyl-terminated oligo(dimethylsiloxane) ($M^R_2D_8$, $n=8$) were kindly provided by Shin-Etsu Chemical Co. Ltd. MPC was synthesized by the method previously described and purified by recrystallization from acetonitrile [23].

Hydroxy-terminated poly(vinylmethylsiloxane-co-dimethylsiloxane)s (HO–PV_lD_mMS–OH) were synthesized by conventional ring-opening polymerization of cyclosiloxane compounds using KOH (20 ppm) as a catalyst (Scheme 1). The molecular weight of hydroxy-terminated silicones was controlled by changing the ratio of D and $M^R_2D_8$. The ratio of D^V_4 and D_4 was adjusted at 1/9 in every case. The synthetic condition is summarized in Table 1. The absolute molecular weight (M_w)

Table 1
Synthetic results of hydroxy-terminated poly(dimethylsiloxane-co-vinylmethylsiloxane) (OH–PV_lD_mMS–OH)

Code	$M^R_2D_8/(Me_2SiO)_4/(MeViSiO)_4$ (mol)	Me_2SiO/MeViSiO (molar fraction)		M_w ($\times 10^4$)	M_w/M_n
		In feed	In copolymer[a]		
OH–$PV_{17}D_{173}$MS–OH	1/37/5	0.89/0.11	0.91/0.09	1.43[b]	1.16[b]
OH–$PV_{32}D_{324}$MS–OH	1/82/10	0.89/0.11	0.91/0.09	2.68[b]	1.16[b]
OH–$PV_{53}D_{537}$MS–OH	1/172/20	0.90/0.10	0.91/0.09	4.44[c]	–

[a] Determined by ^{1}H NMR.
[b] Absolute molecular weight: determined by MALLS.
[c] Calculated from apparent molecular weight.

of the HO–PV_lD_mMS–OH was determined by size-exclusion chromatography equipped with multiangle laser light scattering (SEC-MALS) analysis with a Shodex KF-806L column and a Wyatt Dawn HELEOS detector. The apparent molecular weights of the HO–PV_lD_mMS–OH were also measured using gel-permeation chromatography (GPC) through a Shodex KF-803 column using a calibration curve based on linear polystyrene standards. THF was used as the GPC solvent.

To obtain a macromolecular chain transfer agent (macro-CTA), DCC (4.0 molar to HO–PV_lD_mMS–OH) in CH_2Cl_2 (100 mL) was added dropwise to a CH_2Cl_2 (100 mL) solution of 4-cyanopentanoic acid dithiobenzoate (2.4 molar to HO–PV_lD_mMS–OH) and HO–PV_lD_mMS–OH (30 g) and stirred for 20 h at 40 °C (Scheme 2). The solution was then filtered to remove any insoluble substances. After evaporation of CH_2Cl_2, the reaction mixture was washed with methanol until the methanol was colorless, diluted with chloroform, washed three times with brine, dried over $MgSO_4$, and concentrated. A viscous liquid was obtained. The chemical structure of macro-CTA was confirmed by ^{1}H NMR (α-500, JEOL, Tokyo, Japan) and FT-IR spectroscopy (FT-500, Jasco, Tokyo, Japan). ^{1}H NMR (500 MHz, $CDCl_3$): δ = macro-CTA: −0.2 to 0.2 (m; Si–CH_3), 1.9 (s; CN–C–CH_3), 2.35–2.75 (m; –C–CH_2–CH_2–COOH), 5.6–5.8 (m; –CH=CH_2), 5.8–6.0 (m; –CH=CH_2), 7.3–7.9 (m; Ph).

2.2. Synthesis of block copolymers

Because the radical for polymerization was sensitive to air, all reactions were performed in an argon gas atmosphere. The synthetic condition of the block copolymers is summarized in Table 2. Typically, α,α′-azobisisobutyronitrile (AIBN, 0.025 mmol) was introduced through a polymerization tube. MPC (4.43 g, 15.0 mmol) and macro-CTA ($PD_{324}V_{32}$MS, 0.05 mmol) were desorbed in a toluene/ethanol (1/1) mixture, and the volume of the solution was adjusted to 30 mL. Then, argon gas was passed through the solution for 30 min to eliminate oxygen. The solution was heated at 70 °C and stored with gentle shaking for given periods. After polymerization, the block copolymer was precipitated into THF, then dissolved in ethanol, and again precipitated into THF. The precipitation was dried *in vacuo*. The synthetic route of the PMPC–PV_lD_mMS–PMPC triblock copolymers is shown in Scheme 3.

The number- and weight-averaged molecular weights of the block copolymers were measured with a Tosoh GPC system with a refractive index detector and size-exclusion columns, Shodex, SB-804 HQ and SB-806M HQ with a poly(ethylene glycol) (PEG, Tosoh standard sample) standard in 20 vol.% methanol containing 10 mM LiBr. The molar fraction of the MPC unit of block copolymer was also determined by phosphorus analysis.

2.3. Preparation of silicone substrate and surface functionalization

Silpot 184 PDMS prepolymer was mixed thoroughly with its cross-linking catalyst (10:1, w/w) and poured into a Petri dish. After the bubbles were removed from the prepolymer under reduced pressure, the films were cured at 100 °C for 3 h. The cured film was removed from the plate and cut into 1.4 cm diameter disks. The film disks were washed thoroughly with hexane

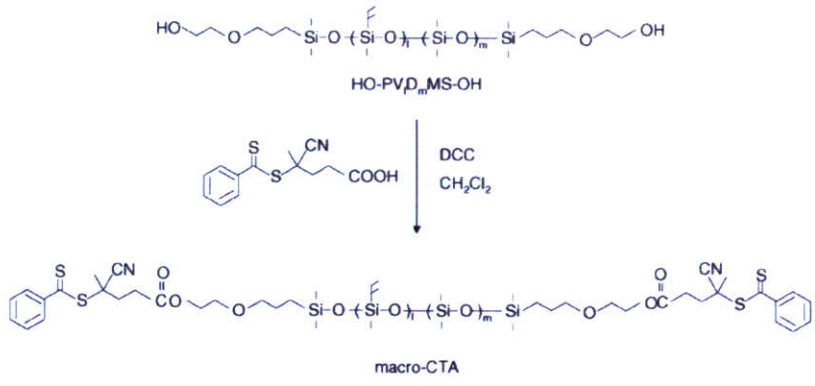

Scheme 2. Synthetic route of macro chain transfer agent (macro-CTA).

Table 2
Synthetic results of PMPC–PV$_l$D$_m$MS–PMPC triblock copolymers

Code	Copolymers	MPC/macro-CTA/AIBN (mol) in feed[a]	PMPC$_{PD(one\ side)}$ in copolymer[b]	M_w ($\times 10^4$)[c]	M_w/M_n	PMPC/silicone[d]
26–173	PMPC$_{26}$–PV$_{17}$D$_{173}$MS–PMPC$_{26}$	$1.5\times 10^{-2}/1\times 10^{-4}/5\times 10^{-5}$	26.0	2.32	1.27	0.27
35–173	PMPC$_{35}$–PV$_{17}$D$_{173}$MS–PMPC$_{35}$	$1.5\times 10^{-2}/5\times 10^{-5}/2.5\times 10^{-5}$	34.7	3.53	1.31	0.37
53–173	PMPC$_{53}$–PV$_{17}$D$_{173}$MS–PMPC$_{53}$	$1.5\times 10^{-2}/2.5\times 10^{-5}/1.25\times 10^{-5}$	52.7	6.85	1.41	0.55
54–324	PMPC$_{54}$–PV$_{32}$D$_{324}$MS–PMPC$_{54}$	$1.5\times 10^{-2}/1\times 10^{-4}/5\times 10^{-5}$	54.2	3.93	1.28	0.30
66–324	PMPC$_{66}$–PV$_{32}$D$_{324}$MS–PMPC$_{66}$	$1.5\times 10^{-2}/5\times 10^{-5}/2.5\times 10^{-5}$	66.3	6.23	1.41	0.37
119–324	PMPC$_{119}$–PV$_{32}$D$_{324}$MS–PMPC$_{119}$	$1.5\times 10^{-2}/2.5\times 10^{-5}/1.25\times 10^{-5}$	118.6	9.85	1.63	0.66
75–325	PMPC$_{75}$–PV$_{53}$D$_{537}$MS–PMPC$_{75}$	$1.5\times 10^{-2}/1\times 10^{-4}/5\times 10^{-5}$	75.3	8.47	1.47	0.26
99–537	PMPC$_{99}$–PV$_{53}$D$_{537}$MS–PMPC$_{99}$	$1.5\times 10^{-2}/5\times 10^{-5}/2.5\times 10^{-5}$	99.2	11.30	1.55	0.34
153–537	PMPC$_{153}$–PV$_{53}$D$_{537}$MS–PMPC$_{153}$	$1.5\times 10^{-2}/2.5\times 10^{-5}/1.25\times 10^{-5}$	152.2	16.64	1.63	0.52

[a] [MPC] = 0.5 mol/L; [CTA]/[AIBN] = 2; polymerization temperature 70 °C; solvent: ethanol/toluene = 1/1 (v/v).
[b] Determined by phosphorus analysis, PD: polymerization degree.
[c] Determined by GPC, eluent: MeOH/H_2O = 20/80 with 10 mM LiBr.
[d] $n\times 2/(l+m)$, PMPC$_n$–PV$_l$D$_m$MS–PMPC$_n$.

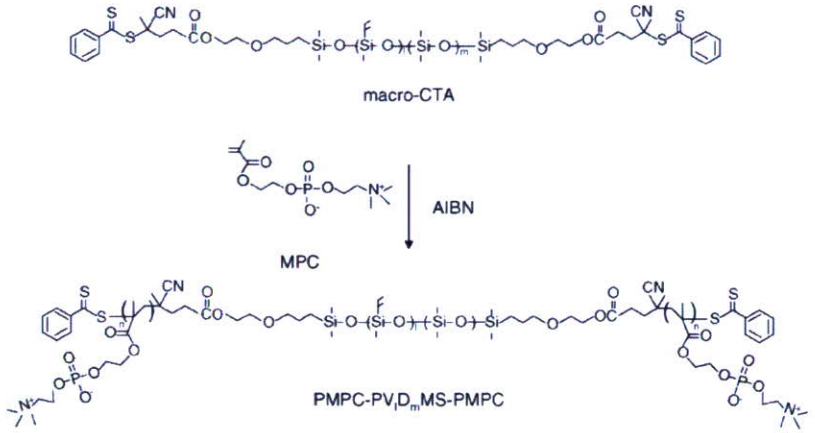

Scheme 3. Synthetic route of PMPC–PV$_l$D$_m$MS–PMPC triblock copolymer.

and acetone and dried under *in vacuo* for 1 day at room temperature. The surface functionalization of the PDMS films was processed as previously described [37]. Briefly, the silicone films were incubated in a solution of poly(hydromethylsiloxane) (KF-99-P®):2-propanol (3:5, v/v) containing triflic acid as a catalyst (0.02 mL) with stirring for 15 min at room temperature. The silicone films were then removed from the solution and washed thoroughly with 2-propanol and hexane, then dried *in vacuo* for 1 day at room temperature. The presence of surface Si–H groups (absorption peak at 2167 cm^{-1}) was confirmed by ATR-FT-IR.

2.4. Surface modification of silicone films with PMPC–PV$_l$D$_m$MS–PMPC triblock copolymer

A solution (5 g) of 1 wt% PMPC–PV$_l$D$_m$MS–PMPC triblock copolymers desorbed in ethanol was prepared and Pt-catalyst (platinum–divinyltetramethyldisiloxane complex) (two drops) was added to the polymer solution. The solution was dropped onto a Si–H functionalized silicone film and spin-coated at 4000 rpm for 10 s. The film was heated at 80 °C for 2 h, then rinsed by soaking in ethanol for 24 h at 50 °C. The ethanol was changed several times. The film was then dried *in vacuo*. Fig. 1 is a schematic representation of the surface modification of PDMS with PMPC–PV$_l$D$_m$MS–PMPC triblock copolymers.

2.5. Surface analysis

X-ray photoelectron spectroscopy (XPS) was performed on a Scienta ESCA-200 spectrometer with Al Kα. Survey scans

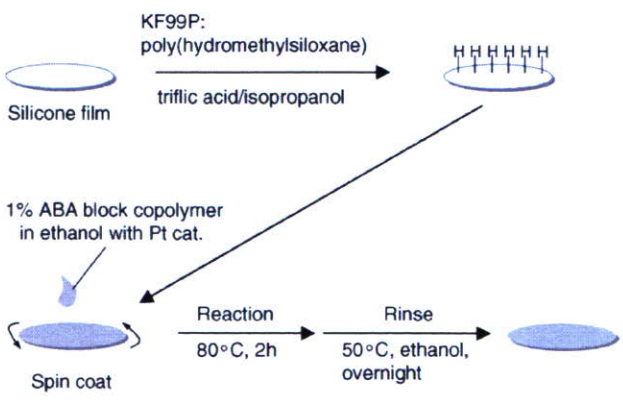

Fig. 1. Schematic representation of surface modification of PDMS with PMPC–PV$_l$D$_m$MS–PMPC triblock copolymer.

spectra of C 1s, O 1s, N 1s, and P 2p were obtained. All XPS data were collected at take off angles of 75° (between the specimen surface and the detector).

The dynamic contact angles for the samples were recorded as the probe fluid, water (deionized to 18.2 MΩ), using a First Ten Angstroms FT-125 goniometer and Gilmont syringes. The advancing (θ_A) and receding (θ_R) contact angles were measured with addition to and withdrawal from the drop, respectively.

The surface frictional coefficients during startup and under steady state conditions were measured using a surface property tester (Heidon Type32, Shinto Science Co., Tokyo, Japan). Sample films ($\phi = 1.4$ cm) were thoroughly wet with water before and during the measurements. The measurements were conducted by sliding the membrane under a 100 g load using a stainless steel ball (10 mm in diameter). The scan speed and scale were 10 mm/s.

2.6. Platelet adhesion test

Human platelet-rich plasma (PRP) was prepared from citrated whole blood by centrifugation. Polymer samples were placed in a 24-well tissue culture plate and secured with a silicone rubber ring. The PBS was allowed to stand in the wells overnight to equilibrate the surface. PRP was poured into each well and stored at room temperature for 60 min. The polymer surfaces in contact with PRP were observed by a scanning electron microscope (S-3400NX, Hitachi High-Technologies Co., Tokyo, Japan). The density of adherent platelets was determined by measuring lactic acid dehydrogenase (LDH) from the platelets [38]. After the PRP was incubated on the polymer samples, the samples were rinsed three times with PBS. The samples were then transferred to a new 24-well tissue culture plate. Triton X-100 (0.5 wt%, 1 mL) was introduced into each well and incubated for 30 min. The Triton X-100 solution (250 μL) was collected and the concentration of LDH from the adherent platelets was measured by the LDH-Cytotoxic Test kit (Wako Pure Chemical Industries, Ltd., Japan).

2.7. Controlled protein adsorption on surface patterned with UV-light irradiation

UV light ($\lambda = 185$ nm) (GL15ZH, Sankyo Denki Co. Ltd., 15 W) was irradiated on a poly(hydromethylsiloxane)-treated PDMS surface through a mesh used for transmission electron microscopy (hole 45 μm, bar 40 μm; Okenshoji Co. Ltd., Tokyo, Japan) for 3 h in air. The UV-irradiated surfaces were then immobilized with the triblock copolymer (119–324) mentioned above.

The surface was exposed to 0.45 g/dL fluorescein isothiocyanate (FITC)-labeled bovine albumin (Sigma Chemicals, St. Louis, MO, USA) in phosphate-buffered solution (PBS) for 30 min and rinsed with PBS and water. The sample was dried in an argon stream and observed using a fluorescent microscope (IX-70, Olympus Co., Tokyo, Japan).

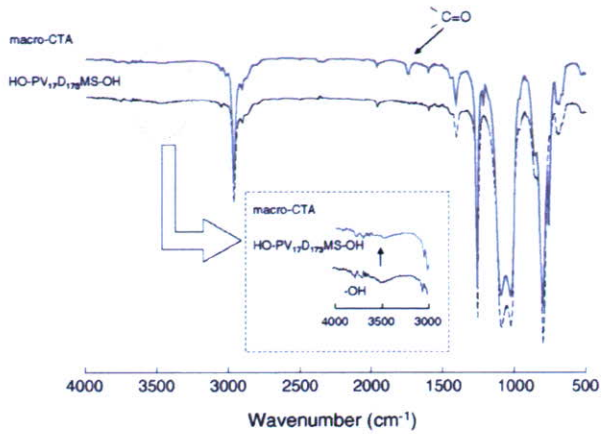

Fig. 2. IR spectra of $PV_{17}D_{173}MS$ and macro-CTA.

3. Results and discussion

3.1. Synthesis of triblock copolymers

Hydroxy-terminated poly(dimethylsiloxane) copolymers (HO–PV_lD_mMS–OH) were synthesized by ring-opening polymerization of cyclotetrasiloxane compounds (Scheme 1). The ratio of dimethylsiloxane and vinylmethylsiloxane in the copolymer could be controlled by their ratio in the feed. The molecular weight of the synthesized silicone compounds was measured by SEC-MALS. For HO–$PV_{17}D_{173}$MS–OH and HO–$PV_{32}D_{324}$MS–OH, the absolute molecular weights were $(1.43 \text{ and } 2.68) \times 10^4$, respectively. Their ratio of apparent molecular weight measured by GPC to absolute molecular weight was 1.4. The absolute molecular weight of HO–$PV_{53}D_{537}$MS–OH was calculated at 4.44×10^4 from the apparent molecular weight. The molecular weight of HO–$PV_{53}D_{537}$MS–OH increased linearly ($r^2 = 0.99$) with an increase in the monomer ratio to $M_2^R D_8$.

4-Cyanopentanoic acid dithiobenzoate, that is, the RAFT agent was reacted with the HO–PV_lD_mMS–OH by condensation. Fig. 2 shows the FT-IR spectra of HO–PV_lD_mMS–OH and that reacted with the 4-cyanopentanoic acid dithiobenzoate. After the reaction, absorption due to the carbonyl group at 1750 cm^{-1} was observed. The absorption of the hydroxyl group at 3500 cm^{-1} diminished. Quantitative determination of the condensation was performed by ^1H NMR. In every case, the composition of the RAFT agent was approximately 2 when the molecular weight of the silicone compound determined by SEC-MALS was used.

Living radical polymerization has a great deal of synthetic power in controlling the molecular architecture of polymers and is an exceptionally robust method for producing block or graft copolymers [28,39–41]. The living radical polymerization of MPC recently resulted in the preparation of biocompatible block [35,42–45] and graft copolymers [46,47].

While Ma et al. firstly synthesized a series of diblock and triblock copolymers of PMPC and oligodimethylsiloxane *via* ATRP, the characterization of the block copolymers was not described in detail because of the solubility

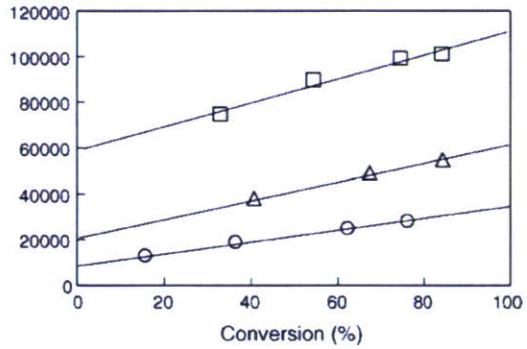

Fig. 3. Dependence of M_w on conversion in the polymerization of MPC: (○) PMPC–$PV_{17}D_{173}$MS–PMPC; (△) PMPC–$PV_{32}D_{324}$MS–PMPC; (□) PMPC–$PV_{53}D_{537}$MS–PMPC.

difference of the components [42]. We also tried to synthesize macro-initiator for ATRP. However, the decrease in the molecular weight of HO–PV_lD_mMS–OH was observed when HO–PV_lD_mMS–OH was reacted with 2-bromoisobutyryl bromide.

RAFT polymerization of MPC with RAFT agent-capped silicone as a dithioester chain transfer agent (macro-CTA) was then performed in toluene/ethanol (1/1) at 70 °C. Even though macro-CTAs have vinyl groups as side chains, any gelation during polymerization was not observed. Fig. 3 shows the relationship between the molecular weight determined by GPC and the conversion of the MPC polymers. In every polymer system, the GPC results show a single peak and the molecular weight of the block copolymer is linear with conversion. Fig. 4 shows that the monomer consumption followed first order kinetics. The semi-logarithmic plot indicates that polymerization is first order with respect to MPC and implies that the polymer radical concentration remains constant on the polymerization time scale. Table 2 summarizes the characterization of PMPC–PV_lD_mMS–PMPC triblock copolymers with various chain lengths. The degree of polymerization (PD) of the MPC polymer increased with an increase in the ratio of MPC to macro-CTA. The yield of polymerization related with polymerization kinetics and increased with an increase in the molecular weight of macro-CTA. The molecular weight distributions were relatively larger with the

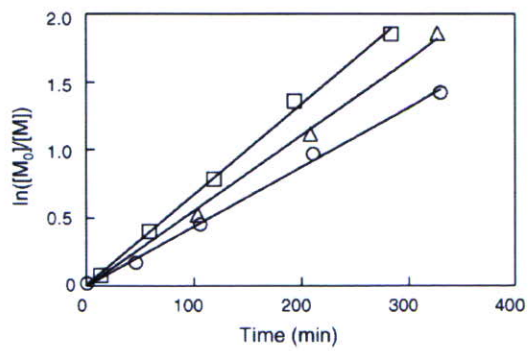

Fig. 4. Kinetics of RAFT polymerization of MPC: (○) PMPC–$PV_{17}D_{173}$MS–PMPC; (△) PMPC–$PV_{32}D_{324}$MS–PMPC; (□) PMPC–$PV_{53}D_{537}$MS–PMPC.

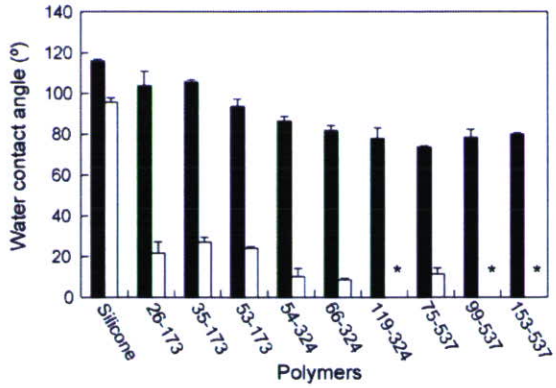

Fig. 5. Water contact angles of native silicone film and that coated with block copolymers: (■) advancing contact angle (θ_A); (□) receding contact angle (θ_R). * represents spreading of water drop.

higher molecular weights. The ratio of MPC and silicone units was calculated from the phosphorus analysis data. When $PV_{32}D_{324}$MS was used as macro-CTA, the composition of the MPC units in a copolymer was higher than that of other macro-CTAs.

3.2. Surface modification and characterization of PDMS with triblock copolymers

All copolymers were dissolved in ethanol and coated on silicone films. The water contact angle data was recorded using specimens dried for several hours under reduced pressure before measurement (Fig. 5). The data for the native PDMS was $\theta_A/\theta_R = 116°/96°$ and did not change by treatment with poly(hydromethylsiloxane). The θ_A on the surface coated with the triblock copolymers was recorded at the first addition of water and it gradually decreased with an increase in the composition of the MPC unit in the copolymers. The θ_R on the modified surface was decreased dramatically to less than 30°. Particularly, the θ_R on a surface coated with copolymers (119–324, 99–537, and 153–537) could not be measured because the water drop spread completely.

The elemental analyses of the polymer-coated silicone surfaces were performed with XPS. In the case of a silicone film coated with the triblock copolymer (66–324), nitrogen and phosphorus peaks were observed at 402.5 and 134.0 eV, respectively (Fig. 6). These were not observed on the native silicone film and were attributed to the phosphorylcholine group in the MPC units. To affect the chemical reaction of surface modification, the triblock copolymer was treated without a Pt catalyst or Si–H treatment. In both cases, the phosphorus and nitrogen signals caused by the MPC polymers were negligible. The surface modification with the triblock copolymers was then performed through hydrosilylation. The XPS phosphorus concentration of the surface-modified silicone films is summarized in Fig. 7. The increment of concentration was caused by an increase in the bulk composition of the MPC unit in the triblock copolymers. Although the block copolymer with a longer central silicone chain (153–537) has longer PMPC chains, the XPS phosphorus concentration on the surface coated with 153–537 was less

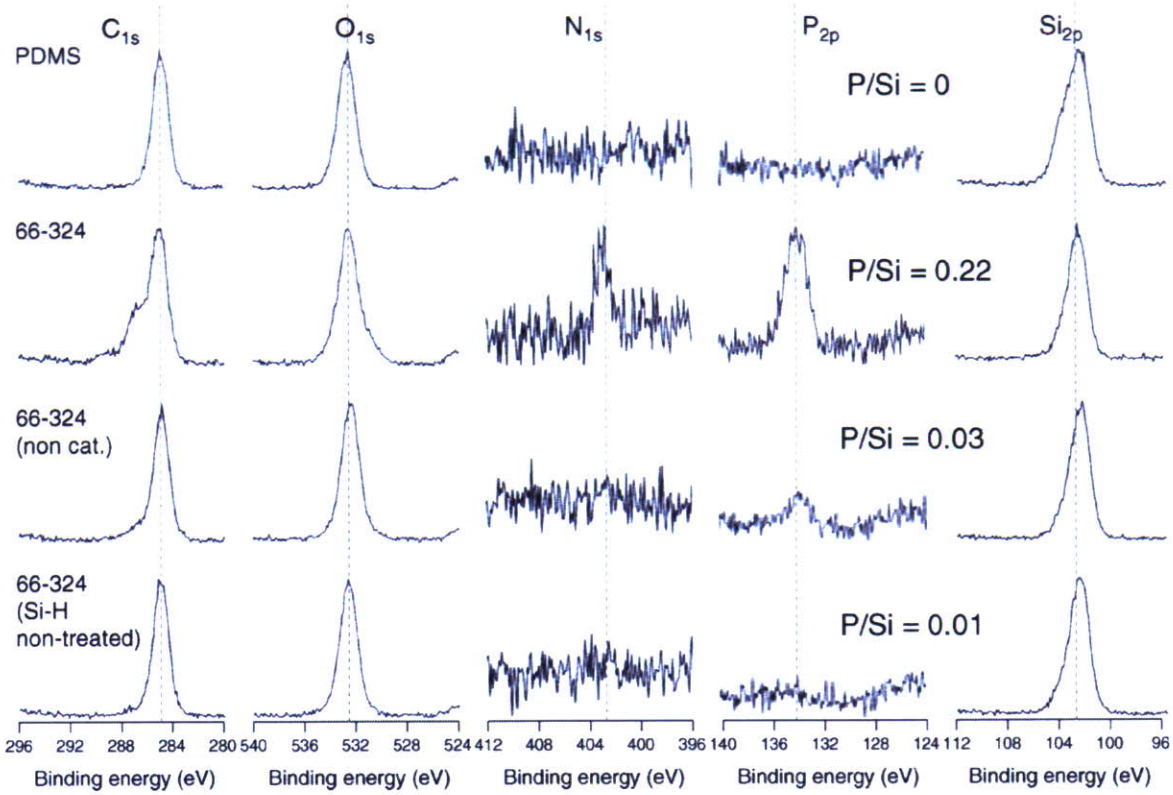

Fig. 6. XPS spectra of native silicone film and that coated with the triblock copolymer (66–324).

than that on the surface coated with 119–324. This result indicates that the central silicone block with high molecular weight reduce the density of PMPC chains on the surface. Sugiyama et al. synthesized poly(MPC-*b*-PDMS) by conventional radical polymerization and surface modification of PDMS with the block copolymer was performed [48]. While the block copolymers improved wettability, the contact angle was still higher than that on comb-shaped polymer brush surface of PMPC [36]. The silicone segments of the block copolymers influenced the mobility of PMPC segments. On the other hand, the PMPC segments of ABA typed block copolymers synthesized in this study were free. Highly wettable surfaces were obtained due to the ABA typed structure.

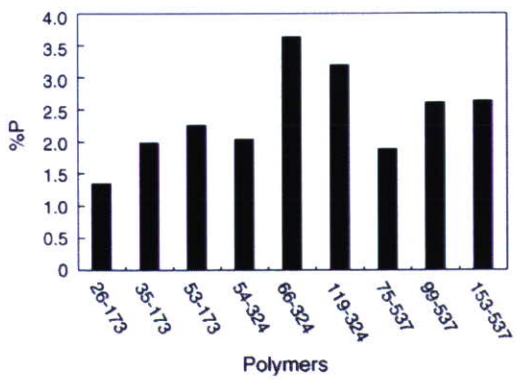

Fig. 7. XPS phosphorus concentration of silicone films modified with PMPC–PV$_l$D$_m$MS–PMPC triblock copolymers.

One of the interesting properties of MPC polymers is to produce lower friction and improved boundary lubrication under wet condition [49] and this property is important for making biomedical devices such as, catheters. To clarify the effect of chemical structure of block copolymers on improving boundary lubrication, we measured surface friction of modified surfaces. Fig. 8 shows the friction coefficient of the silicone films coated with triblock copolymers at startup (static) and in the steady (kinetic) conditions in water. The static and kinetic friction coefficients of non-treated silicone film were coefficient 2.0 ± 0.4 and 1.4 ± 0.3, respectively. These coefficients were significantly reduced by triblock copolymer coatings. The surface friction was decreased with an increase in the ratio of MPC in a copolymer. Even if the 153–537 has long PMPC blocks, the longer silicone block is an obstacle to improve surface lubrication. In the case of the triblock copolymer (119–324)-coated surface, the kinetic friction coefficient was less than 0.01. The surface friction was effectively reduced by coating of optimally sequenced ABA block copolymers as well as "grafting from" typed surface modification [14]. This phenomenon is attributed to the removal of the strong hydrophobic interaction between the PDMS surfaces in water [50] and a similar state of hydrodynamic lubrication.

Moro et al. investigated the effects of the graft polymerization of MPC onto polyethylene surfaces. They clarified that MPC grafting remarkably decreased friction and the amount of wear [51]. The PMPC–PV$_l$D$_m$MS–PMPC triblock copolymers syn-

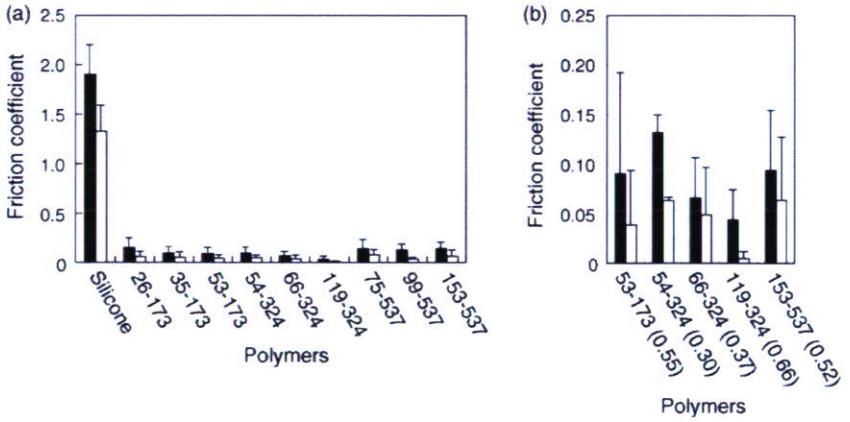

Fig. 8. Friction coefficients of silicone films modified with block copolymers: (■) startup; (□) steady state; (a) all data; (b) selected data for a better reading. The values in parentheses: $n \times 2/(l+m)$, $PMPC_n$–PV_lD_mMS–$PMPC_n$.

thesized in this study can be chemically introduced on various surfaces through the reactivity of the vinyl group in the central silicone chain.

Fig. 9 shows the results of a continuous friction test on a silicone film and that coated with the triblock copolymer (119–324). The low friction coefficient of a surface coated with the triblock copolymer (119–324) did not change during the determination. This result indicates that surface modification with a block copolymer is stable due to chemical bonding to the substrate. The long-term stability of coating layer and the influence of percentage of vinyl unit will be presented in near future.

3.3. Non-fouling behavior on PDMS surface coated with PMPC–PV_lD_mMS–PMPC triblock copolymers

Fig. 10 shows SEM pictures of a polymer surface after contact with human PRP for 60 min. Many platelets adhered and were active on the non-treated silicone surface. In contrast, platelet adhesion was effectively reduced on the PDMS surface coated with the triblock copolymer (119–324). The quantitative result for adherent platelets on various surfaces is summarized in Fig. 11. On every PMPC–PV_lD_mMS–PMPC triblock copolymer-immobilized surface, the number of adherent platelets was significantly smaller than that on a non-treated silicone surface. Moreover, platelet adhesion was significantly decreased on the surface coated with 119–324 compared to that coated with 153–537, that is, the surface density of PMPC chains also influenced non-fouling properties. The suppression of platelet adhesion on the block copolymer-coated surfaces is due to the reduction of plasma protein adsorption. In the former literatures [23,24,52], the mechanism of protein adsorption resistance on MPC polymers has been well reported and the property was observed regardless of type of protein. The reduction of albumin adsorption on the surface coated with a triblock copolymer is presented in Fig. 12.

Surface modification with well-defined MPC polymers on a solid surface produced by living radical polymerization has been chiefly reported by Feng et al. [53]. The effect of thickness and density of the PMPC polymer on protein adsorption is also well characterized [54]. Surface samples with various graft densities from 0.06 to 0.39 chains/nm^2 and chain lengths from 5 to 200 MPC units were prepared. They clarified that the surfaces with high graft densities and high PMPC chain lengths showed dramatic reductions in fibrinogen adsorption. A well-defined surface structure bearing a free end of the polymer chain must be advantageous for obtaining the efficiency of MPC polymers on non-fouling phenomena. The PMPC–PV_lD_mMS–PMPC triblock copolymer is suitable for fabricating this surface structure by a simple coating process.

Adsorption of FITC-labeled BSA was well controlled on a patterned polymer surface, as shown in Fig. 12. In the region

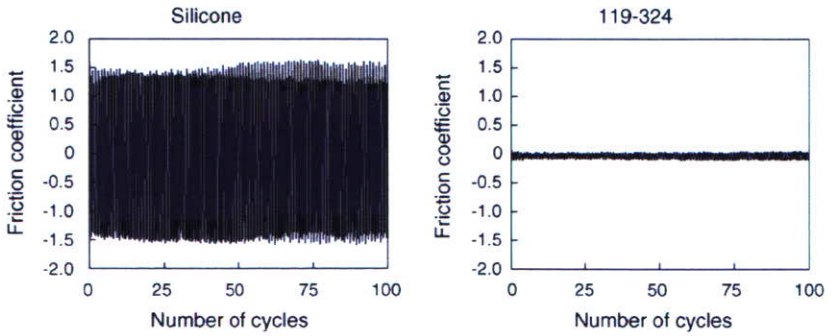

Fig. 9. Continuous friction test for a silicone film and that coated with the triblock copolymer (119–324).

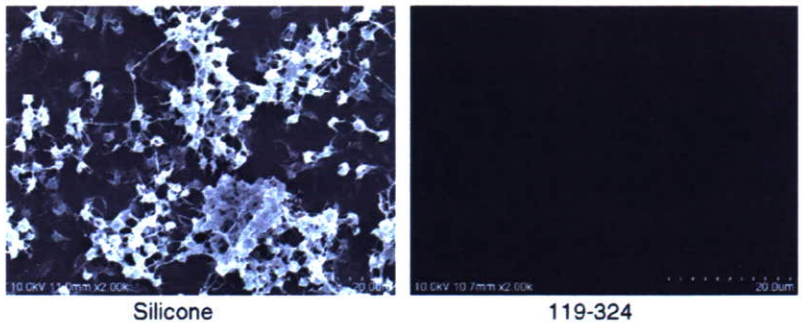

Fig. 10. SEM pictures of polymer surfaces after contact with PRP for 60 min.

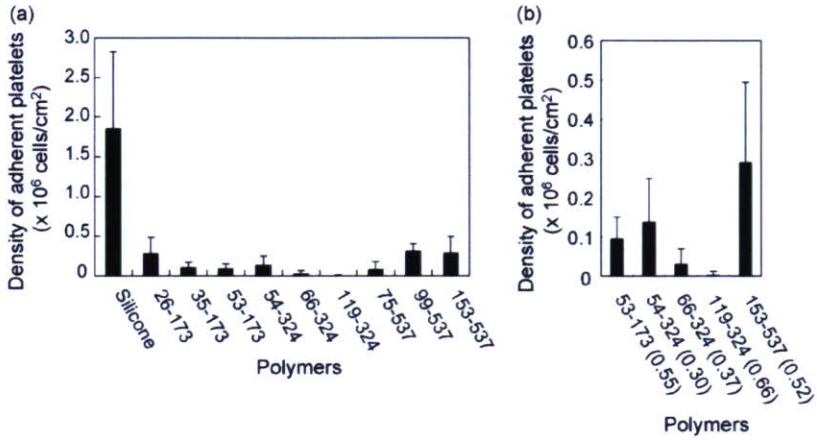

Fig. 11. Surface density of adherent platelets on polymer surfaces in contact with PRP for 60 min: (a) all data; (b) selected data for a better reading. The values in parentheses: $n \times 2/(l+m)$, $PMPC_n$–PV_lD_mMS–$PMPC_n$.

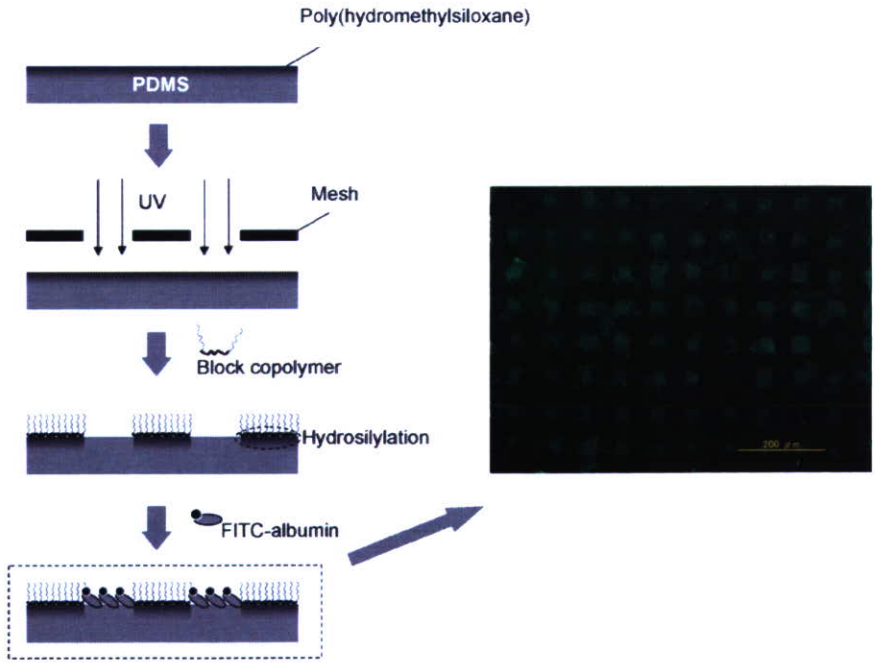

Fig. 12. FITC-albumin adsorption on PDMS surface coated with the triblock copolymer (119–324) with micropatterning after contact with 0.45 g/dL FITC-albumin in PBS for 30 min.

irradiated with UV, no Si–H bond was determined by ATR-FT-IR (data not shown). Fig. 6 shows that surface modification is performed *via* hydrosilylation, that is, Si–H bond is required on the substrate surface. The triblock copolymer (119–324) selectively reacted with the non-UV-irradiated region. The intensity of the surface fluorescence of the UV-irradiated region was significantly high. This indicates that a large amount of BSA was adsorbed on this region. In contrast, BSA adsorption was effectively reduced on the region covered with mesh. The protein adsorption behavior confirmed that the surface modification with block copolymers was performed thorough hydrosilylation. The surface modification with ABA block copolymers can prepare highly defined micropatterns and their potential applicability to biosensor and drug screening development will be demonstrated.

4. Conclusion

For the surface modification of PDMS, PMPC–PV$_l$D$_m$MS–PMPC triblock copolymers were synthesized *via* RAFT polymerization. Polymerization of each unit was well controlled and the molecular weight distribution was relatively low. The rate of copolymerization of MPC depends on the molecular weight of the macro-CTA. The copolymers were coated on PDMS and chemically bonded *via* hydrosilylation. The surface wettability of the copolymer-immobilized surface was significantly improved compared with that of native PDMS. Copolymers are very effective in reducing the coefficient of friction of the surface. Platelet adhesion and protein adsorption on the PDMS surface coated with triblock copolymers was reduced dramatically. To optimize the sequence of block copolymers is very important because the surface properties coated with the block copolymers depend on both the molecular weight and density of PMPC chains, and RAFT polymerization well works to achieve this process. We also succeeded in controlling the size of the modification area on a microscale and in manipulating protein adsorption on the surface.

Acknowledgments

This work was supported by the Japan Society for the Promotion of Science (Grant-in-Aid for Encouragement of Young Scientists (#18681018)). We gratefully acknowledge the valuable discussions provided by Dr. Kazuhiko Ishihara of The University of Tokyo and Mr. Masayuki Ikeno of Shin-Etsu Chemical Co. Ltd.

References

[1] J. Curtis, A. Coals, in: B.D. Ratner, A.S. Hoffman, F.J. Schoen, J.E. Lemons (Eds.), Biomaterials Science, 2nd ed., Elsevier Academic Press, San Diego, 2004 (Chapter 7).
[2] J.C. McDonald, D.C. Duffy, J.R. Anderson, D.T. Chiu, H. Wu, O.J. Schueller, G.M. Whitesides, Electrophoresis 21 (2000) 27.
[3] J. Soo Ko, H.C. Yoon, H. Yang, H.B. Pyo, K. Hyo Chung, S. Jin Kim, Y. Tae Kim, Lab Chip 3 (2003) 106.
[4] R.G. Lammertink, S. Schlautmann, G.A. Besselink, R.B. Schasfoort, Anal. Chem. 76 (2004) 3018.
[5] M. Ebara, J.M. Hoffman, A.S. Hoffman, P.S. Stayton, Lab Chip 6 (2006) 843.
[6] W.J. Kao, Q.H. Zhao, A. Hiltner, J.M. Anderson, J. Biomed. Mater. Res. 28 (1994) 73.
[7] M.C. Belanger, Y. Marois, J. Biomed. Mater. Res. 58 (2001) 467.
[8] C. Leunisse, R. van Weissenbruch, H.J. Busscher, H.C. van der Mei, F. Dijk, F.W. Albers, J. Biomed. Mater. Res. 58 (2001) 556.
[9] C. Price, M.G. Waters, D.W. Williams, M.A. Lewis, D. Stickler, J. Biomed. Mater. Res. 63 (2002) 122.
[10] M. Morra, E. Occhiello, F. Garbassi, M. Maestri, R. Bianchi, A. Zonta, Clin. Mater. 5 (1990) 147.
[11] S.L. Peterson, A. McDonald, P.L. Gourley, D.Y. Sasaki, J. Biomed. Mater. Res. 72 (2005) 10.
[12] S. Hu, X. Ren, M. Bachman, C.E. Sims, G.P. Li, N. Allbritton, Anal. Chem. 74 (2002) 4117.
[13] Y. Yuan, X. Zang, F. Ai, J. Zhou, J. Shen, S. Lin, Polym. Int. 53 (2004) 121.
[14] T. Goda, T. Konno, M. Takai, T. Moro, K. Ishihara, Biomaterials 27 (2006) 5151.
[15] C.-G. Golander, J.N. Herron, K. Lim, P. Claesson, P. Stenius, J.D. Andrade, in: J.M. Harris (Ed.), Poly(ethylene glycol) Chemistry, Plenum Press, New York, 1992 (Chapter 15).
[16] A. Papra, N. Gadegaard, N.B. Larsen, Langmuir 17 (2001) 1457.
[17] A. Papra, A. Bernard, D. Juncker, N.B. Larsen, B. Michel, E. Delamarche, Langmuir 17 (2001) 4090.
[18] E. Delamarche, C. Donzel, F.S. Kamounah, H. Wolf, M. Geissler, R. Stutz, P. Schmidt-Winkel, B. Michel, H.J. Mathieu, K. Schaumburg, Langmuir 19 (2003) 8749.
[19] C. Donzel, M. Geissler, A. Bernard, H. Wolf, B. Michel, J. Hilborn, E. Delamarche, Adv. Mater. 13 (2001) 1164.
[20] D. Wu, B. Zhao, Z. Dai, J. Qin, B. Lin, Lab Chip 6 (2006) 942.
[21] X. Fan, L. Lin, P.B. Messersmith, Biomacromolecules 7 (2006) 2443.
[22] K. Ishihara, T. Ueda, N. Nakabayashi, Polym. J. 22 (1990) 355.
[23] Y. Iwasaki, A. Mikami, K. Kurita, N. Yui, K. Ishihara, N. Nakabayashi, J. Biomed. Mater. Res. 36 (1997) 508.
[24] K. Ishihara, H. Nomura, T. Mihara, K. Kurita, Y. Iwasaki, N. Nakabayashi, J. Biomed. Mater. Res. 39 (1998) 323.
[25] G.H. Hsiue, S.D. Lee, P.C. Chang, C.Y. Kao, J. Biomed. Mater. Res. 42 (1998) 134.
[26] K. Yao, X.D. Huang, X.J. Huang, Z.K. Xu, J. Biomed. Mater. Res. 78A (2006) 684.
[27] S. Lee, J. Voros, Langmuir 21 (2005) 11957.
[28] K. Matyjaszewski, T.P. Davis, Handbook of Radical Polymerization, Wiley–Interscience, Hoboken, 2002.
[29] J.-S. Wang, K. Matyjaszewski, J. Am. Chem. Soc. 117 (1995) 5614.
[30] T.E. Pattern, J. Xia, T. Abernathy, K. Matyjaszewski, Science 272 (1996) 866.
[31] K. Matyjaszewski, J. Xia, Chem. Rev. 101 (2001) 2921.
[32] M. Kamigaito, T. Ando, M. Sawamoto, Chem. Rev. 101 (2001) 3689.
[33] M. Arotcüaréna, B. Heise, S. Ishaya, A. Laschewsky, J. Am. Chem. Soc. 124 (2002) 3787.
[34] Y. Mitsukami, M.S. Donovan, A.B. Lowe, C.L. McCormick, Macromolecules 34 (2001) 2248.
[35] S. Yusa, K. Fukuda, T. Yamamoto, K. Ishihara, Y. Morishima, Biomacromolecules 6 (2005) 663.
[36] R. Iwata, P. Suk-In, V.P. Hoven, A. Takahara, K. Akiyoshi, Y. Iwasaki, Biomacromolecules 5 (2004) 2308.
[37] H. Chen, Z. Zhang, Y. Chen, M.A. Brook, H. Sheardown, Biomaterials 26 (2005) 2391.
[38] L.J. Suggs, J.L. West, A.G. Mikos, Biomaterials 20 (1999) 683.
[39] K. Matyjaszewski, J. Xia, Chem. Rev. 101 (2001) 2921.
[40] J. Pyun, K. Matyjaszewski, Chem. Mater. 13 (2001) 3436.
[41] A. Favier, M.T. Charreyre, Macromol. Rapid. Commun. 27 (2006) 653.
[42] Y. Ma, Y. Tang, N.C. Billingham, S.P. Armes, A.L. Lewis, A.W. Lloyd, J.P. Salvage, Macromolecules 36 (2003) 3475.

[43] Y.T. Li, Y.Q. Tang, R. Narain, A.L. Lewis, S.P. Armes, Langmuir 21 (2005) 9946.
[44] J. Du, Y. Tang, A.L. Lewis, S.P. Armes, J. Am. Chem. Soc. 127 (2005) 17982.
[45] Y. Inoue, J. Watanabe, S. Yusa, K. Ishihara, J. Polym. Sci. Pol. Chem. 43 (2005) 6073.
[46] Y. Iwasaki, K. Akiyoshi, Macromolecules 37 (2004) 7637.
[47] Y. Iwasaki, K. Akiyoshi, Biomacromolecules 7 (2006) 1433.
[48] K. Sugiyama, K. Shiraishi, K. Okada, O. Matsuo, Polym. J. 31 (1999) 883.
[49] J.R. Foy, P.F. Williams III, G.L. Powell, K. Ishihara, N. Nakabayashi, M. LaBerge, Proc. Inst. Mech. Eng. [H] 213 (1999) 5.
[50] S. Lee, N.D. Spencer, Tribo. Int. 38 (2005) 922.
[51] T. Moro, Y. Takatori, K. Ishihara, T. Konno, Y. Takigawa, T. Matsushita, U.I. Chung, K. Nakamura, H. Kawaguchi, Nat. Mater. 3 (2004) 829.
[52] K. Ishihara, N.P. Ziats, B.P. Tierney, N. Nakabayashi, J.M. Anderson, J. Biomed. Mater. Res. 25 (1991) 1397.
[53] W. Feng, J.L. Brash, S. Zhu, J. Polym. Sci. Pol. Chem. 42 (2004) 2931.
[54] W. Feng, J.L. Brash, S. Zhu, Biomaterials 27 (2006) 847.